Lithium isotope behaviour during basalt weathering experiments amended with organic acids

Philip A.E. Pogge von Strandmann[1,2*], Xianyi Liu[2], Chun-Yao Liu[2], David J. Wilson[2], Samantha J. Hammond[3], Gary Tarbuck[2], Ludmilla Aristilde[4], Alexander J. Krause[2], Wesley T. Fraser[5]

[1]Institute of Geosciences, Johannes Gutenberg University, 55122 Mainz, Germany.

[2]London Geochemistry and Isotope Centre (LOGIC), Institute of Earth and Planetary Sciences, University College London and Birkbeck, University of London, Gower Place, London, WC1E 6BS, UK.

[3]School of Environment, Earth and Ecosystems Sciences, The Open University, Walton Hall, Milton Keynes, MK7 6AA, UK.

[4]Department of Civil and Environmental Engineering, McCormick School of Engineering and Applied Science, Northwestern University, USA.

[5]Department of Geography, Oxford Brookes University, Oxford, OX3 0BP, UK.

*Corresponding author: ppoggevo@uni-mainz.de

Abstract

Lithium (Li) isotopes are a tracer of silicate weathering processes, but how they react to different components of organic and plant-assisted weathering is poorly known. To examine the effect of organic acids compared to a strong mineral acid (HCl) on Li isotope behaviour, basalt-water weathering experiments were amended with different organic acids (glycine, malic acid, cinnamic acid, and humic acid; 0.01M). The presence of the different acids

significantly affects the behaviour of dissolved elemental concentrations (such as Mg, Fe, and Al), both by increasing primary rock dissolution and hindering rates of secondary mineral formation. However, the behaviour of Li isotopes appears unaffected, with all experiments following an almost identical trend of δ^7Li versus Li/Na. This observation was consistent with a single fractionation factor during the uptake of Li into secondary minerals, yet both calculated saturation states and leaching experiments on the reacted solids indicated that Li was removed into multiple phases, suggesting that the bulk combined fractionation factor barely varied. Of the Li lost from solution in the organic experiments, we estimated that on average 76% went into neoformed clays, 16% into oxides/oxyhydroxides, and 10% into the exchangeable fraction. The fractionations observed for each phase were $\Delta^7Li_{exch\text{-}soln}$ = -12.7 ± 1.7‰, $\Delta^7Li_{ox\text{-}soln}$ = -26.7 ± 0.4‰, and $\Delta^7Li_{clay\text{-}soln}$ = -21.6 ± 3.3‰. These fractionations were identical, within error, to those from experiments with organic-free water, implying that the Li isotope behaviour was unaffected by the presence of organic acids in the weathering reaction. This result has interesting consequences for the interpretation of Li isotopes in terms of plant-assisted weathering and the geological record of terrestrialisation. In particular, it appears to imply that seawater Li isotope records can be expected to resolve the integrated effect of plants on weathering fluxes or weathering congruence, rather than being sensitive to specific organic-mediated weathering mechanisms.

1.0 Introduction

Chemical weathering of silicate rocks is one of the dominant controls on both long-term climate, via the burial of marine carbonate (Berner et al., 1983; Walker et al., 1981),

and short-term climate, via the delivery of nutrients and clay minerals for the growth and burial of organic carbon in coastal oceans (Kennedy and Wagner, 2011; Lalonde et al., 2012; Ma et al., 2014). As such, significant efforts have gone into understanding and quantifying chemical weathering fluxes in the present day, and the timing and consequences of weathering changes in the geological past.

Lithium (Li) isotopes are a promising tracer of silicate weathering (Tomascak et al., 2016). Because Li is sourced overwhelmingly from silicates rather than carbonates (Kisakürek et al., 2005), and only silicate weathering sequesters carbon dioxide (CO_2) on long timescales, Li isotopes only trace the process that is of relevance to the long-term carbon cycle. In general, there also appears to be no major biological effect on Li isotopes arising from primary productivity (Pogge von Strandmann et al., 2016). There are conflicting reports on whether plants cause Li isotope fractionation (Li et al., 2020), or not (Clergue et al., 2015; Lemarchand et al., 2010), or indeed whether the dissolved load is the primary source of plant-borne Li, or whether the exchangeable fraction is a more important source (Steinhoefel et al., 2021). However, due to the minor amount of Li in plants, they are unlikely to have a resolvable effect on the Li isotope composition of surface waters at a catchment scale. Instead, the wide range in δ^7Li values reported for the dissolved load of rivers (2–44‰; Dellinger et al., 2015; Huh et al., 1998; Murphy et al., 2019) compared to primary silicate rocks (MORB: 3–5‰; continental crust mean: 0.6 ± 0.6‰; Elliott et al., 2006; Sauzéat et al., 2015) is due to fractionation occurring during the silicate weathering process. Rocks are generally dissolved with little to no isotope fractionation (Pistiner and Henderson, 2003; Wimpenny et al., 2010b). Secondary minerals that form during the weathering process (clays, oxides, zeolites) preferentially take up the light Li isotope (^{6}Li), driving residual waters isotopically heavy (Chan et al., 1992; Huh et al., 2001; Kisakürek et al., 2005;

Pogge von Strandmann et al., 2006). In river waters, Li isotopes are therefore controlled by the ratio of primary mineral dissolution relative to secondary mineral formation (e.g. Dellinger et al., 2015; Pistiner and Henderson, 2003; Pogge von Strandmann et al., 2010; Vigier et al., 2009). A predominance of primary mineral dissolution (i.e. congruent weathering) will drive solution δ^7Li values towards the composition of the rock (i.e. low δ^7Li), whereas increasing secondary mineral formation (i.e. incongruent weathering), relative to primary mineral dissolution, will increase solution δ^7Li values (Dellinger et al., 2015; Pogge von Strandmann and Henderson, 2015; Pogge von Strandmann et al., 2017). Lithium isotopes therefore inform on weathering regimes, which affect CO_2 drawdown efficiency (due to retention of cations such as Ca or Mg in secondary minerals) during both the present and the geological past.

While a fairly significant body of research now exists on Li isotopes and weathering in modern rivers, soils, and groundwaters (see summaries in Penniston-Dorland et al., 2017; Pogge von Strandmann et al., 2020; Pogge von Strandmann et al., 2021a; Tomascak et al., 2016), relatively fewer low-temperature laboratory experiments have been conducted (Hindshaw et al., 2019; Li and Liu, 2020; Pistiner and Henderson, 2003; Pogge von Strandmann et al., 2019b; Vigier et al., 2008; Wimpenny et al., 2010b; Wimpenny et al., 2015; Zhang et al., 1998). However, such experiments are important for quantifying the direct controls of the different aspects of weathering (e.g. pH, temperature, rock surface area, organic acids) on Li isotopes.

An important stage in the development of chemical weathering during the Phanerozoic was the evolution and expansion of land plants, known as terrestrialisation (Algeo and Scheckler, 1998; Algeo and Scheckler, 2010; Berner, 1998; Kenrick, 2003; Kenrick et al., 2012). Plants influence chemical weathering processes and rates in several different

97 ways (Algeo and Scheckler, 1998; Beerling and Berner, 2005; Berner et al., 2003). Roots can
98 physically break up primary rock, which increases the surface area for chemical weathering
99 (Dontsova et al., 2020), and enhance rock dissolution via the exudation of organic acids
100 (Golubev et al., 2006; Welch and Ullman, 1993). However, plants can also help to bind and
101 consolidate soils, thereby helping to protect them against physical erosion (Gibling and
102 Davies, 2012), while at the same time potentially enhancing the formation of secondary
103 minerals (Jackson, 2015). Several studies have suggested that terrestrialisation caused
104 significant global increases in chemical weathering, leading to an increased drawdown of
105 atmospheric CO_2, and potentially triggering cold periods and mass extinctions in the
106 Devonian-Carboniferous (Berner, 1998, 2006; Dahl and Arens, 2020; Lenton et al., 2018;
107 Lenton et al., 2012).

108 A recent study that reconstructed seawater Li isotope compositions for the past 3 Ga
109 revealed an intriguing increase in δ^7Li values starting in approximately the mid-Palaeozoic
110 (Kalderon-Asael et al., 2021). This increase has been attributed to the combined effect of
111 terrestrialisation, and the evolution of more Si biomineralisers changing oceanic reverse
112 weathering. In particular, terrestrialisation appears to have promoted the formation of
113 secondary minerals on the continents. It is therefore important to resolve whether plants
114 have a direct effect on solution Li isotopes by changing partition coefficients and isotopic
115 fractionation factors, or only an indirect effect by changing weathering fluxes and
116 congruence.

117 In this study we present the results of multiple basalt-water weathering experiments
118 that were carried out with the addition of different organic acids. We compare them to
119 previous 'inorganic' basalt-water experiments (Pogge von Strandmann et al., 2019b) that

used the same rock and water, with the aim of assessing the direct impact on Li isotope fractionation of plant-induced weathering (and hence terrestrialisation).

2.0 Methods

2.1 Experimental methods

The inorganic water-rock experiment reported in Pogge von Strandmann et al. (2019) followed the earlier experiments of Jones et al. (2012). Approximately 250 g of basaltic sand from the Hvitá estuary (Borgarfjörður) in western Iceland was reacted for over eight months with 900 ml of water (from the Great Ouse River in eastern England) at 20°C in a shaking bath reactor. Water samples (of 50 ml) were taken periodically, via a 0.2 μm pore size syringe filter, and stored in pre-cleaned HDPE containers.

The experiments reported here were conducted at the same time, using the same rock and water, but with the addition of organic acids of different complexity to the water. All experimental solutions were made up at 0.01M concentration, to match both other organic acid experiments (e.g. Gudbrandsson et al., 2014; Jones, 1998; Welch and Ullman, 1993), and also to fit within the range observed in natural systems (e.g. Adeleke et al., 2017). The simplest organic acid used was glycine (NH_2-CH_2-COOH), which is also the simplest amino acid. Next most complex is the carboxylic acid cinnamic acid (C_6H_5CH=CHCOOH), which occurs in a number of plants, including the *Cinnamomum* genus. Malic acid is yet more complex, and is a dicarboxylic acid ($C_4H_6O_5$) produced by all organisms. The final organic acid used was humic acid, which is often produced in organic-rich soils. Humic acid(s) are a much larger molecule than the others used here, and have a significantly more complex structure. In order to compare the effects of organic acids to an

143 inorganic mineral acid (Welch and Ullman, 1993), an experiment was also run with 0.01M
144 HCl.
145 Following the experiments, the reacted basalt was dried and compared to the
146 original unreacted basalt, by examining the exchangeable, oxide/oxyhydroxide, and clay
147 fractions, as well as the bulk rock. The exchangeable fraction was obtained following the
148 Tessier method, by leaching the basalt in 1 M sodium acetate for 1 h at room temperature
149 (Li et al., 2020; Pogge von Strandmann et al., 2013; Pogge von Strandmann et al., 2019a;
150 Pogge von Strandmann et al., 2021b; Pogge von Strandmann et al., 2019b; Tessier et al.,
151 1979; Tsai et al., 2014). Na acetate was used, rather than other reagents such as $MgCl_2$, due
152 to the low lithium blanks of Na acetate. To preferentially leach oxides and oxyhydroxides,
153 the material was then leached in 0.04M hydroxylamine hydrochloride (HH) in 25% (v/v)
154 acetic acid for 1 h at room temperature (Hindshaw et al., 2018; Jiang et al., 2007; Li et al.,
155 2020; Wilson et al., 2013). Finally, the residue was leached for 1 h in 0.6 M HCl, which
156 attacks the secondary mineral fraction, i.e. clays, as well as any remaining oxyhydroxides
157 and zeolites, but also potentially any primary silicates (Pogge von Strandmann et al., 2019b;
158 Pogge von Strandmann et al., 2014). The bulk basalt was dissolved using a standard method
159 of concentrated HF-HNO_3-$HClO_4$, followed by concentrated HNO_3 and 6 M HCl.
160
161 *2.2 Concentration analyses*
162 Solution concentrations were analysed at The Open University, using an Agilent 8800
163 triple quadrupole inductively coupled plasma mass spectrometer (ICP-MS). The instrument
164 has two quadrupole mass filters, which are separated by a collision/reaction cell (allowing
165 targeted interference removal in the cell). We ran in two modes of analysis: no-gas for Li (as
166 no interfering ions are present on mass) and in He collision mode for all other analytes. In

no-gas mode, oxide levels (measured as CeO^+/Ce^+) were 0.96% and doubly-charged species (Ce^{2+}/Ce^+) were 1.80%. In He mode, these were 0.44% and 1.30%, respectively.

Prior to analysis, samples were diluted 10-fold from the original solutions in 2% HNO_3 to allow analysis of all masses in the same analytical session. Analyses were calibrated against a suite of synthetic multi-element solutions. An on-line internal standard (Rh and In) was added to each sample and standard to monitor and correct for instrumental drift, and to check for any undue ionisation effects from the different acid matrices. Where concentrations were above the detection limit in the initial water, reproducibility was better than 2.5% (relative standard deviation from the mean of the five measurements). Accuracy was determined using the international river water reference standard SLRS-5, which was within uncertainty of certified values. Lithium and silicon are not certified in SLRS-5, so in this case we compared to published concentrations, which were also within uncertainty (Heimburger et al., 2013).

Major elemental concentrations of the starting basalt are published (Jones et al., 2012), except for Li concentrations, which were determined by ICP-MS analyses in a similar manner to the dissolved concentrations. We analysed BCR-2 as an external standard, which gave values within uncertainty (± 6%) of Li concentrations in BCR-2 determined previously by isotope dilution (Pogge von Strandmann et al., 2011). The elemental ratios of the leachates were determined using a Varian 720ES ICP-OES. Samples were calibrated using matrix-matched synthetic standards (i.e. in Na acetate, HH, and dilute HCl).

2.3 Li isotope analyses

The analytical methods for Li isotopes are described in previous publications (Pogge von Strandmann et al., 2011; Pogge von Strandmann et al., 2019b). Briefly, 15ml of water

was dried down and then purified using a two-stage cation exchange method, using dilute HCl as an eluent. Analyses were performed on a Nu Instruments Plasma 3 MC-ICP-MS, by bracketing the samples with concentration-matched IRMM-016. Samples were then re-normalised to the L-SVEC standard [although the isotope ratios of the two standards are effectively identical (Jeffcoate et al., 2004; Pogge von Strandmann et al., 2019b)], and errors were propagated through the correction. The accuracy and precision for analyses of seawater (δ^7Li = 31.18 ± 0.38‰, 2sd, n=29) and BCR-2 basalt (δ^7Li = 2.64 ± 0.31‰, n=7) compare well to other studies (Jeffcoate et al., 2004; Li et al., 2020; Pogge von Strandmann et al., 2011; Pogge von Strandmann et al., 2019b).

3.0 Results

3.1 pH behaviour

The pH of the filtered river water used to make up the initial solutions was 6.8. The evolution of solution pH in the different experiments is shown in Figure 1 and Table 1. The addition of the different acids caused different effects on pH, compared to the basalt-water experiments detailed in Pogge von Strandmann et al. (2019). Some experiments (e.g. glycine) had little pH variation during the experiment, while others (e.g. malic acid and even HCl) exhibited significant pH changes (Fig. 1).

3.2 Major elemental concentrations

The elemental concentrations during the reaction between river water and the basalt were detailed in Pogge von Strandmann et al. (2019). Briefly, major elements like Mg and Si increased due to the dissolution of the basalt, with Mg concentrations increasing by a factor of ~1.5. In the experiments reported here, the Mg concentrations always increase

through time, but by different amounts (Fig. 2a, Table 1). The next smallest increase is for the humic acid experiment (1.6×), followed by cinnamic acid (1.7×), glycine (1.8×), HCl (2.9×), and finally malic acid (6×). Silicon shows a broadly similar pattern of increases (Fig. 2b), except that the greatest increase is for the HCl experiment, with the malic acid results tracking the HCl experiment for the first few days but finishing at a lower level similar to the humic acid. Overall, the major element data suggested that primary basaltic minerals are dissolving during these experiments, and that both inorganic and organic acids are enhancing the dissolution in comparison to the simple water-rock experiment.

3.3 Aluminium, iron and lithium concentrations

Aluminium concentrations are fairly variable in the different experiments, although all show an increase in concentration (Fig. 2c). Several of the organic acid experiments display much higher concentrations within the first few days, followed by a decline over several months. Iron concentrations exhibit patterns similar to those of Al (Fig. 2d), except that in the HCl experiment, [Fe] decreases with time, while [Al] does not.

In contrast to most other elements, Li concentrations decreased by a factor of ~10 in the normal water-rock experiment (Pogge von Strandmann et al., 2019), similar to the behaviour observed in other basaltic experiments (Jones et al., 2012). In all the organic experiments, there is also a decrease in Li concentrations following a similar pattern, but to a variable and lesser degree (Fig. 3a). The HCl experiment displays a different behaviour, with an increase by a factor of 1.3 in Li concentrations (Fig 3a), similar to the major element behaviour. To summarise the last two sections, the elemental concentration behaviour of the organic acid experiments is broadly similar in terms of general trends for each element

238 to the simple water-rock experiments, but with varying degrees of enrichment or depletion
239 and more anomalous behaviour for malic acid.
240
241 *3.4 Leachate concentrations*
242 While sequential leaches are never completely efficient at recovering the phase of
243 interest (Pogge von Strandmann et al., 2019b), the elemental ratios indicate that the
244 leaches have largely targeted the correct phases (Table 2). For example, Li/Si ratios are
245 several orders of magnitude higher in the exchangeable fraction than in the bulk basalt,
246 while Mg/Si and Ca/Si are also higher in the exchangeable fraction. Si (as a neutral species)
247 should not be dominantly associated with the exchangeable fraction, while both Mg and Ca
248 are known to be affected by sorption (Pogge von Strandmann et al., 2012; Tipper et al.,
249 2021); as such these results support the reliable extraction of an exchangeable fraction.
250 Higher Mg/Si in the pre- compared to post-reaction exchangeable fraction (by an average
251 factor of 2.8) suggests that the natural water the basaltic sand was originally in had a slightly
252 different Mg/Si composition compared to the experimental water. However, different
253 elemental ratios between these phases are not observable in the exchangeable fraction for
254 other elements. The oxide/oxyhydroxide fraction has up to 20 times higher Fe/Si ratios than
255 the bulk unreacted rock (Table 2), and up to 30 times higher Al/Si ratios. That fraction also
256 has similar to, or higher, Li/Si ratios than clays, indicating that Li is incorporated into
257 oxyhydroxides to a relatively greater extent than Si. However, the Li/Si in the exchangeable
258 fraction is highest, confirming that Si is barely adsorbed. In the HCl leach targeting clays,
259 Li/Si ratios are orders of magnitude lower than in the exchangeable fraction, but
260 approximately an order of magnitude higher than in the unreacted basalt. In other words, Si
261 is a significant element in clay minerals, and the leachates appear to be reflecting this.

Overall, the elemental ratios of the different experiments are broadly the same for each leach type and indicate that the leaches have dominantly attacked the target phases.

3.5 Mineral saturation indices

Mineral saturation was calculated using the PHREEQC programme, with a combination of its standard thermodynamic database, plus the THERMODDEM and MINTEQ databases (Merkel and Planer-Friedrich, 2005; Parkhurst and Appelo, 1999). The Minteq v4 and NIST4.2 databases also contains thermodynamic data for most of the relevant organic acids. However, at the experimental concentration of 0.01M, these acids make no difference to the calculated SI values. The chemical compositions of the solutions were consistently undersaturated with respect to the primary basaltic minerals, such as forsterite, albite, and Mg-rich pyroxenes, indicating that they had a tendency to dissolve. However, the secondary mineral saturation indices were more variable, as detailed in Figure 4. In general, the HCl and early part of the malic and humic acid experiments were undersaturated for many secondary minerals, such as smectite and Fe- and Al- oxyhydroxides. In contrast, the higher pH experiments tended towards supersaturation of such secondary minerals (Fig. 4).

3.6 Lithium isotope compositions

The bulk unreacted basalt and the bulk basalt after each experiment effectively had the same δ^7Li composition of 3.9 ± 0.4‰ (1sd). The pre-experiment exchangeable fraction had a δ^7Li value of 17.8‰, and 21.3–21.8‰ after the simple water-rock reaction (Pogge von Strandmann et al., 2019b). The HCl experiment had an exchangeable fraction with a δ^7Li value of 2.6‰, but all organic acids had exchangeable fractions of 16.8–21.6‰ (Table 2). The oxyhydroxide fractions have much lower δ^7Li values: 3.7‰ in the unreacted basalt,

286 5.5‰ after water-rock experiments, -4.0‰ for the HCl experiment, and 2.8–8.0‰ for the
287 organic acid experiments. Finally, the HCl leach that should target clays has a δ^7Li value of
288 5.3‰ in the original basalt and 4.8‰ in the HCl leach, but 9.3–10.8‰ in the water-rock
289 experiments and 6.6–10.7‰ in the organic acid experiments. Hence, overall, each fraction
290 has similar compositions in both the simple water-rock and organic experiments, which are
291 generally different from values in the HCl experiment and the bulk basalt.
292 As shown in Figure 3b, the solution δ^7Li values increase with reaction time, aside from the
293 HCl experiment, which stays broadly constant. The final values, and the pattern and rate of
294 δ^7Li increase, varies somewhat across the different organic acid experiments. Thus, all the
295 organic experiments had a final δ^7Li value within 5.6‰ of each other, although some
296 organic experiments, notably humic acid, may not have reached a full steady-state for Li
297 isotopes by the end of the experiment. We note that in the original water-rock experiments,
298 two identical experiments were conducted and ended with δ^7Li values within 0.08‰ of each
299 other (Pogge von Strandmann et al., 2019b). Hence, a variability of 5.6‰ is far outside of
300 the likely within-experiment variability.
301
302 **4.0 Discussion**
303 *4.1 Basaltic rock dissolution*
304 In all the experiments, the concentrations of Na, Mg, and Si in solution increase with
305 time, with the simple water-rock experiments exhibiting the lowest increases (Fig. 2; Table
306 1). Interestingly, the HCl experiment displays the greatest concentration increases for Si and
307 Na, while the largest concentration increases for Mg are seen in the malic acid experiment
308 by a factor of 6, compared to a factor of 1.5 in the water-rock experiment. Aside from the
309 malic acid, all other experiments approximately follow the stoichiometric dissolution of

basalt when plotting Mg against Si concentrations (Fig. 5a), which indicates largely congruent dissolution for these major elements. Malic acid, which is well known for Mg-malate complexation and can thus enhance Mg leaching out of the surface layers of the basaltic minerals, is likely responsible for the high Mg concentrations in the experiment with malic acid (Adeleke et al., 2017; Dontsova et al., 2014; Uysal et al., 2018; Wang et al., 2005).

Therefore, for all experiments except the one with malic acid, it appears that Mg and Si concentrations can be used to estimate the amount of basalt dissolved during the duration of the experiment, given the apparent lack of significant removal of Mg and Si into secondary phases. This approach is also supported by the evolution of solution Mg/Si ratios during the experiments, which decreased from the composition of the starting water towards that of basalt. Thus, compared to the dissolution of 15–70 mg of basalt during the water-rock experiments (where the lower number in each case is based on Si concentrations, and the higher number on Mg concentrations), the amount of dissolved basalt increased to 40–100 mg for the glycine, cinnamic, and humic acid experiments, and to 200–270 mg for the HCl experiment. For the malic acid experiment, due to the likelihood of Mg-malate complexation (discussed further below), we use Si concentrations to estimate the amount of basalt dissolved and find it was similar to most of the other organic acid experiments (50 mg).

It has been shown that silicate dissolution rates are higher at lower pH (as well as at alkaline pH>10) (Brady and Walther, 1989). However, with the addition of organic material at near-neutral pH, organic acids also promote dissolution (Welch and Ullman, 1993). Both these behaviours were observed here; for example, Si concentrations were highest at low pH values, while at near-neutral pH, the organic acid experiments had higher Si concentrations than the inorganic water-rock experiments (Fig. 6a). However, Welch and

Ullman (1993) also showed that dissolution rates in organic acid solutions can be up to 10 times higher than in inorganic acid solutions (HCl) at the same pH. Such a result was not seen in our experiments, although the Welch and Ullman (1993) experiments were conducted on plagioclase, and our material is only 11% plagioclase (Jones et al., 2012). In any case, the HCl experiments clearly exhibited a greater dissolution than most of the organic acid experiments at the same pH (Fig. 6).

4.2 Element stoichiometry

In most cases the bulk basalt appears to be dissolving stoichiometrically (except for the malic acid experiment for Mg) for major elements such as Mg (Fig. 5a), Na (Fig. 5e), and Si. Some small deviations are occasionally observed (Fig. 5), and this may be due to preferential dissolution of individual mineral phases. However, stoichiometry is in general not followed for solution trace elements such as Al, Fe, or indeed Li (Fig. 5b–d). Such incongruent behaviour for Al and Fe is not unexpected, as it is well documented that this can happen, due to changes in sorption and complexation (Dontsova et al., 2014; Sposito, 2008). In general, the degree of complexation depends on the organic acid involved (primarily the number of carboxyl groups), the type of metal and its concentration, and the pH of the solution (Ganor et al., 2009; Jones, 1998). For example, malate strongly complexes to Fe at low pH, but significantly less so at near-neutral pH, where Fe-oxyhydroxide precipitation can occur (Jones, 1998; Stefansson and Gislason, 2001). Such pH-dependent complexation could therefore explain the decrease in dissolved Fe concentrations as pH increases (from pH ~6.6 to 6.9) in the malic acid experiment (Fig. 2d, 6b), in combination with greater silicate secondary mineral formation at higher pH (Stefansson and Gislason, 2001). In contrast, there is no obvious pH control on Li abundance, since experiments with

358 different pH values have similar Li concentration ranges (e.g. cinnamic and humic acids
359 compared to water and glycine; Fig. 6c).
360 Based on the Li/Mg and Li/Si ratios of the unaltered, pre-experimental basalt, and
361 assuming congruent dissolution, we calculated the amount of Li added to solution from
362 basalt dissolution in each experiment. In all cases, except for the HCl experiment, the
363 amount of Li added by dissolution is only 4–6% of the Li removed during the experiment by
364 the formation of secondary minerals (discussed below), and is therefore insignificant. In the
365 case of HCl, the solution Li concentration increased with time (Fig. 3a).
366 Overall, while Mg versus Si plots indicate generally stoichiometric dissolution of the
367 bulk basalt (aside from the Mg-malate complexation; Fig. 5a), none of the experiments
368 follow stoichiometry in Li versus Si plots (Fig. 5b). Aside from the HCl experiment, all
369 experiments lose Li relative to Si. In the HCl experiment, such Li release is likely due to
370 preferential leaching of certain minerals within the basalt. For example, basaltic glass
371 dissolves more easily and has a higher Li/Si than other basaltic minerals (Sonntag, 2007). For
372 the other experiments, decreases in Li concentrations are likely driven by secondary mineral
373 formation, which is discussed in detail below.
374
375 *4.3 Mineral stability and saturation*
376 Mineral stability fields were calculated using PhreePlot, which is a programme that
377 couples with PHREEQC. As such, the same thermodynamic databases were used as for the
378 saturation index calculations. When calculating mineral stability fields (plotted in Na^+/H^+
379 versus H_4SiO_4 space), the experiments all plot within the hematite stability field, which
380 reflects the high saturation index of hematite (and other Fe oxides and hydroxides) towards
381 the end of all experiments (Fig. 4b and 4c). We note that the addition of organic acids (via

382 the databases mentioned above) at a concentration of. 0.01M did not change the nature or
383 location of the stability fields. Equally, all experiments apart from the one with HCl are
384 mostly supersaturated for gibbsite (Fig. 4d). The malic acid experiment is unusual. It is
385 undersaturated at low pH (rather like the HCl experiment) at the beginning of the
386 experiment, but evolves towards a saturation state and pH that are similar to the water-
387 rock experiment by the end. As described above, the high supersaturation of the malic acid
388 experiment is likely due to Al- (as well as Fe and Mg) malate complexation at low pH
389 (Dontsova et al., 2014).

390 Interestingly, the saturation indices of hematite, as well as more poorly crystalline
391 Fe-oxyhydroxides such as ferrihydrite and lepidocrocite, correlate well with pH, both overall
392 and within individual experiments (Fig. 4b, e, f), with high pH waters (5.8–7.8) being most
393 supersaturated. In contrast, secondary minerals such as smectite (Fig. 4a), gibbsite (Fig. 4d)
394 and kaolinite exhibit more scatter. In other words, while the degree of saturation of Fe
395 oxyhydroxide is strongly correlated with pH in these experiments, the saturation state of
396 secondary minerals containing Al are not well-correlated with pH.

397 In order to examine the stability of other secondary minerals, we also calculated
398 mineral stability fields excluding hematite (Fig. 7). In this case, the water-rock experiment
399 plots within the Mg-smectite (Montmorillonite-Aberdeen) stability field, which agrees with
400 the correlation observed between the saturation index of this mineral and δ^7Li values
401 reported in the previous study (Pogge von Strandmann et al., 2019b). However, the organic
402 acid experiments plot within different stability fields (bearing in mind that all are also within
403 the hematite field). The malic acid experiment is largely within the Ca-smectite field, while
404 humic acid plots mainly within the kaolinite field. The glycine experiments cross the

boundary between goethite and Mg-smectite, while the cinnamic acid experiment is largely in the goethite field.

In general, however, these differences in mineral stability do not appear to be reflected in the behaviour of elements such as Al or Fe. For example, the Al/Fe ratio of the solutions barely change as the stability field boundaries are crossed (e.g. the cinnamic acid experiment starts with an Al/Fe of 2.59, and finishes with a ratio of 2.63). A switch from goethite to Al-silicate secondary minerals should cause a dramatic change, even allowing for the fact that hematite likely dominates the Fe budget (e.g. a shift from 80% hematite, 10% goethite and 10% gibbsite, to 80% hematite and 20% goethite, would theoretically cause the molar Al/Fe to change from 0.06 to 0.13). One possibility is that a significant number of different secondary minerals are precipitating throughout all the experiments, thereby somewhat buffering the major and trace element behaviour. Such buffering may also be true for Li isotope behaviour, as discussed below.

4.4 Lithium mass balance

Constructing a mass balance for Li between the different solid phases allows the determination of the destination of the Li that was lost from the experimental fluids. The selective leaches that were employed (Pogge von Strandmann et al., 2019a; Pogge von Strandmann et al., 2019b; Pogge von Strandmann et al., 2014; Tessier et al., 1979) allow three different destinations to be distinguished: the exchangeable fraction (i.e. sorbed Li), the oxide fraction (i.e. Li in Fe, Mn, and Al-oxyhydroxides, where the HH method likely leaches poorly crystalline minerals such as ferrihydrite and lepidocrocite (Poulton and Canfield, 2005), as well as amorphous versions of hematite, etc.), and the silicate secondary mineral fraction (i.e. Li substituting into the crystal structures of neoforming minerals such

as clays). For this mass balance we assume that the different leaches solely attack their target phase, and we use the comparison of the leaching of unreacted (pre-experimental) material to reacted material:

$$f_x = -\frac{\left(Li_{post} - Li_{pre}\right)_x}{\left(Li_{post} - Li_{pre}\right)_{soln}}$$

where f_x is the fraction of Li in phase x (exchangeable, oxide or clay), Li is the mass of Li (in g) in the different pre- and post-experimental phase x, and soln is in solution. Loss of material and volume during solution sampling is accounted for in the weights of solution Li, i.e. the product of the Li concentration and the volume of solution remaining. This mass balance has an independent check for accuracy, because the sum of the Li in each of the phases can be compared to that removed from solution. Overall, the sum of Li in each of those phases combined is within 97–108% of the amount of Li removed from solution, meaning that the mass balance appears accurate within this precision (±8%), with the uncertainty arising from analytical and weighing uncertainty, as well as leaching inefficiency.

This mass balance cannot be constructed for the HCl experiment as the solution gains Li, indicating that the solid phases must have lost Li through dissolution. Although selective leaches were performed on the final solid phases, the exchangeable fraction for the HCl experiment contains considerably less Li than the water-rock experiments, by a factor of ~4, and only approximately half as much Li as is in the exchangeable fraction of the initial unreacted basalt (suggesting that some of the original exchangeable Li was released during the experiment). The oxide phase for the HCl experiment contains around half as much Li as the reacted basalt from the water-rock experiments, and around the same amount of Li as the initial unreacted basalt. For the secondary clay fraction, the HCl experiments have about 1.5× less Li than the basalt after the inorganic water-rock reaction,

while they have the same amount of Li as the pre-reaction basalt (Pogge von Strandmann et al., 2019b).

In contrast, all the other experiments lost Li from solution, with 7–12% (10–14% in water-rock experiments) taken up by the exchangeable fraction, 6–23% (17–21% in water-rock) by the oxide fraction (Fig. 8), and the remainder (68–82%) taken up by clays (66–68% in water-rock experiments). These fractions are within the ranges reported for Hawaiian soils, where clays also dominate the budget of removed Li, followed by oxides and then by the exchangeable fraction (Li et al., 2020). In contrast, in sediments from Svalbard and agricultural soil from the UK, the exchangeable fraction dominates over the oxide and clay fractions (Hindshaw et al., 2018; Pogge von Strandmann et al., 2021b), although the latter example was a weathering experiment intentionally run out of steady-state with the artificial addition of fresh olivine. In the organic experiments described here, it generally appears that the experiments with the lowest pH (humic and cinnamic acids) have the highest proportion of Li in the exchangeable and clay fractions (Fig. 9a and 9c), but the lowest proportion in the oxide fraction (Fig. 9b).

The most striking observation is the close correlation between the proportion of Li in the oxide phase and the final pH in each experiment (r^2 = 0.96; Fig. 9b). This relationship likely arises from a pH control on the formation of Fe oxyhydroxides (Stefansson and Gislason, 2001), especially the more poorly crystalline minerals (e.g. ferrihydrite or lepidocrocite) that are more easily leached by the HH method (Poulton and Canfield, 2005), which is supported by the positive co-variation between the fraction of Li in the oxide phase and the saturation index of Fe oxyhydroxide minerals, such as ferrihydrite or lepidocrocite (r^2 = 0.90; not shown). In other words, when Fe oxyhydroxide precipitation is more favourable (i.e. greater supersaturation), there is more Li in the oxide phases, indicating that

476 these phases could be an important sink for Li through co-precipitation. The same co-
477 variations do not exist for Al-oxyhydroxides, such as gibbsite, which may suggest that Li is
478 not partitioning as much into Al-phases. Calculations using PHREEQC suggest that all Mn
479 oxide and Mn oxyhydroxide phases known to that programme are highly undersaturated, so
480 are unlikely to play a role here. There is also a negative co-variation between pH and Li in
481 the clay fraction (r^2 = 0.69), which could indicate a pH-dependence on clay formation but
482 could also simply reflect the counterpart to the Li removal into oxides.
483 To summarise, it appears from these experiments that the uptake of Li into the
484 different solid phases is at least party controlled by the solution pH, likely through its
485 control on the precipitation of Fe oxyhydroxides. Uptake of Li by clays may be weakly
486 dependent on pH, but this is hard to resolve from these experiments.
487
488 *4.5 Lithium isotope fractionation into the solid phases*
489 Assuming that the Li concentrations and isotope compositions measured in the
490 exchangeable, oxide and secondary mineral fractions represent formation from dissolved Li
491 in the youngest (most recent) experimental fluids, it is possible to calculate the fractionation
492 between the fluid and each solid fraction. This assumption may be complicated by Li uptake
493 from earlier on in the experiment, which then becomes isolated from the solution by
494 successive precipitation. As such, the isotopic fractionation observed especially in the fast-
495 reacting exchangeable fraction likely represent a condition at steady-state (possibly
496 equilibrium), which is therefore a minimum $\Delta^7Li_{exch\text{-}soln}$ value. Bulk fractionation factors are
497 also calculated by a different method in Section 4.7.
498 It is also theoretically possible that the Li isotope values were altered by diffusion,
499 because ^6Li diffuses faster than ^7Li (Richter et al., 2003). Generally, this is a high

500 temperature process, but has been reported from experiments at 50–90°C, albeit it some at
501 far-from-equilibrium conditions (Richter et al., 2006; Verney-Carron et al., 2011), and
502 observed at lower temperatures (e.g. Andrews et al., 2020). However, it is unlikely that
503 diffusion is causing significant deviation from isotope fractionation during uptake by
504 secondary minerals, given the constancy in fractionation factor (discussed below).

505 For the exchangeable fraction in the organic experiments, $\Delta^7Li_{exch\text{-}soln}$ varies between
506 -8.5 and -14.9‰, compared to -11.7‰ in the simple water-rock experiments (Fig. 10). The
507 HCl experiment also exhibits fractionation during uptake into the exchangeable fraction of -
508 10‰, although the amount of Li in this phase is considerably smaller than for the other
509 experiments (Table 2). Aside from glycine ($\Delta^7Li_{exch\text{-}soln}$ = -8.5‰), the range of $\Delta^7Li_{exch\text{-}soln}$ is
510 very narrow (average of -12.7 ± 1.7‰ (1sd)). Of all the organic experiments, glycine has the
511 lowest fraction of Li in the exchangeable pool, and the highest in the oxide phase (Fig. 9a
512 and 9b).

513 For the leached oxide fraction, $\Delta^7Li_{ox\text{-}soln}$ is -26.7 ± 0.4‰ (1sd) in the organic acid
514 experiments, compared to –27.8‰ in the water-rock experiments (Fig. 10). Therefore, Li
515 isotope fractionation into the oxide fraction, which is likely predominantly poorly crystalline
516 minerals like ferrihydrite, although amorphous hematite may also be leached, and gibbsite
517 based on the saturation calculations, seems to be unaffected by the presence of organic
518 ligands. The observed fractionation is slightly larger than the fractionation reported for the
519 oxide fraction of marine ferromanganese crusts ($\Delta^7Li_{ox\text{-}soln}$ = -22.3 to +1.5‰ (Chan and Hein,
520 2007)). It is currently unknown why this variability exists, but it could potentially arise from
521 the different solution chemistry (river water vs. seawater), differences in fractionation
522 between different oxide types, or from fractionation during the leaching. However, the
523 similarity of the inferred fractionation across all the experiments (Fig. 10), as well as the

524 reproducibility of sample repeats for the oxide fraction (Table 2), gives us confidence that
525 the method is at least reproducible.

526 There is also little variation in the δ^7Li values of the clay leaches from the organic
527 experiments, which fall in a narrow range of 8.6–10.8‰, leading to a $\Delta^7Li_{clay\text{-}soln}$ of -20.7 to -
528 24.9‰ (average -21.6 ± 3.3‰) (Fig. 10). In comparison, both direct clay mineral synthesis
529 experiments (Hindshaw et al., 2019; Vigier et al., 2008), and primary mineral alteration
530 experiments (Millot et al., 2010; Pogge von Strandmann et al., 2019b; Wimpenny et al.,
531 2010b), report $\Delta^7Li_{clay\text{-}soln}$ values of approximately -20‰ (see also summary in Pogge von
532 Strandmann et al., 2020). In these experiments, although several different types of clay
533 mineral are supersaturated (see above), it may be that the clay mineralogies also consist of
534 amorphous mixtures. Palagonite (the hydrous amorphous alteration product of basaltic
535 glass) or iddingsite (the hydrous amorphous alteration product of olivine) may also be
536 forming, rather than distinct clay types, as demonstrated in some experimental and natural
537 samples (Chemtob et al., 2012; Stefansdottir and Gislason, 2005; Valle et al., 2010).

538 In summary, the isotopic fractionation into the different phases is similar for the
539 simple water-rock experiments and the organic acid experiments, in the order exchangeable
540 < clay < oxyhydroxide (Fig. 10). In terms of the exchangeable fraction and clay
541 neoformation, this result agrees with other experimental observations, where Li isotope
542 fractionation was found to be smaller during uptake by the exchangeable pool (0 to -12‰)
543 than the clay pool (<-21‰) (Chan and Hein, 2007; Hindshaw et al., 2019; Pistiner and
544 Henderson, 2003; Pogge von Strandmann et al., 2020; Pogge von Strandmann et al., 2021b;
545 Pogge von Strandmann et al., 2019b; Vigier et al., 2008; Wimpenny et al., 2010a; Wimpenny
546 et al., 2015). When considering the amount of Li taken up by each phase, the clay fraction
547 dominates the mass budget (Fig. 8). The total mass-balanced Δ^7Li, considering all the

548 secondary phases, varies between –21.7 and -25.4‰ for the different experiments. As such,
549 the overall fractionation is similar to field observations from basaltic soil pore waters and
550 river waters (Liu et al., 2015; Pogge von Strandmann et al., 2021a; Pogge von Strandmann et
551 al., 2010; Pogge von Strandmann et al., 2006; Pogge von Strandmann et al., 2012; Pogge von
552 Strandmann et al., 2016; Vigier et al., 2009).
553
554 *4.6 Lithium isotopes in solution*
555 Aside from the HCl experiment, where Li concentrations increase through time, in all
556 the other experiments the solutions lose Li (Fig. 3A). The simple water-rock experiments lost
557 ~90% of their dissolved Li into secondary phases (Pogge von Strandmann et al., 2019b). For
558 the organic acid experiments, the Li losses are 66–79%. Hence, the addition of organic acids
559 inhibited the overall Li uptake into secondary minerals. This is not simply due to a pH drop
560 from the addition of acids, as demonstrated by the glycine experiments which have a similar
561 pH to the water-rock experiments, but still lose less Li (by 77%). This Li loss is accompanied
562 by Li isotope fractionation, with inverse trends between Li concentration and δ^7Li values
563 (Fig. 3). The addition of Li from congruent basalt dissolution should lead to a decrease in
564 solution δ^7Li values during the experiment, as the basalt has a low isotopic composition (4.4
565 ± 0.4‰ (2sd)). Yet, other than in the HCl experiment, this decrease in δ^7Li values is not seen.
566 Instead, as Li is lost from solution, the solution δ^7Li values increase, indicating that the Li is
567 lost into solid secondary phases that prefer ^{6}Li.
568 While the overall trends are similar between the different organic acid experiments,
569 the rates of increase in δ^7Li values (and the corresponding loss of Li from solution) differ
570 (Fig. 3b). For example, δ^7Li values in the malic acid experiment increased by 3.5‰/month in
571 the first month. In contrast, these numbers are 12.6 ‰/month for the glycine experiment,

572 and 16.5 ‰/month for the water-rock experiments. In other words, while the final values
573 after 250 days only vary by 5.6‰, after 34 days the solution values differ by 13.3‰. This
574 pattern is not replicated in any of the major elemental concentrations, or indeed in Fe or Al
575 concentrations, thus there is no similar pattern in the evolution of secondary mineral
576 saturation. Therefore, even though the Li isotope fractionation factors are broadly similar
577 between all the organic acid experiments (Fig. 10), all organic acids are seen to inhibit the
578 rate of Li uptake by secondary minerals relative to simple water-rock experiments (Ganor et
579 al., 2009).

580 In detail, the overall order from slowest to fastest Li removal after one month (34
581 days) is malic < humic < cinnamic < glycine < water. Interestingly, there is a broadly similar
582 pattern in the solution pH after one month. The three experiments with the least Li removal
583 after one month have a pH of <5, while the two experiments with the most Li removal and
584 most fractionated Li isotopes have a pH >7. In the malic acid experiment, there is little
585 change in Li concentrations or isotopes before one month, with the major increase in δ^7Li
586 values occurring approximately between one and four months (Fig. 3). This interval of Li
587 removal follows a rapid pH increase, from pH 3.3 at the start of the experiment to pH 5.8
588 after one month, before reaching pH 6.4 after four months. Saturation indices for several
589 secondary minerals (Mg-smectite, Fe oxyhydroxides, and to a lesser extent gibbsite) indicate
590 that they were undersaturated at low pH in that experiment, and only reached
591 supersaturation at pH>5 for goethite or pH>5.5 for Mg-smectite (Fig. 4c and 4a
592 respectively), further supporting the importance of the pH control on Li removal.

593 To a first order, it appears that the primary control on secondary mineral formation
594 (and hence Li isotope compositions) is the solution pH, whereby higher pH promotes
595 secondary mineral formation (Stefansson and Gislason, 2001). It is important to note that

596 our organic acid experiments were run under acidic to circumneutral conditions (pH 3.3-
597 7.8). At pH values of 7–10, higher pH generally results in lower smectite (or other silicate
598 secondary mineral) supersaturation in natural waters, so this trend can be expected to be
599 reversed. However, we have too few data in that pH range to constrain such an effect (Fig.
600 4).
601
602 *4.7 Modelling lithium isotope fractionation factors in the presence of organic acids*
603 Solution Li/Na ratios have frequently been used to assess the amount of Li removed
604 from solution into secondary minerals, both in basaltic (Li et al., 2020; Liu et al., 2015; Pogge
605 von Strandmann et al., 2017; Pogge von Strandmann et al., 2016) and other settings
606 (Dellinger et al., 2015; Ma et al., 2020; Pogge von Strandmann et al., 2017). This approach is
607 based on the high solubility and mobility of Na (Gíslason et al., 1996), which means that
608 Li/Na ratios will decrease as Li is removed into secondary minerals relative to Na. As such,
609 many river systems exhibit a negative relationship between δ^7Li and Li/Na ratios (Ma et al.,
610 2020; Murphy et al., 2019; Pogge von Strandmann et al., 2017). Such a relationship also
611 allows isotopic fractionation factors to be determined, based on the assumption that Na is
612 fully mobile, because the use of an elemental ratio circumvents dilution effects (Pogge von
613 Strandmann et al., 2017).
614 The simple water-rock experiments showed a logarithmic relationship between
615 solution Li/Na ratios and δ^7Li values that could be modelled with a Rayleigh-type equation (δ
616 = δ_i + 1000(α-1) $\times$ ln f, where δ and δ_i are the measured and initial delta values, and f is the
617 fraction of Li remaining, converted into a Li/Na ratio assuming that no Na is removed from
618 solution), using a fractionation factor of α = 0.991 (Pogge von Strandmann et al., 2019b),
619 similar to that observed in other basaltic rivers (Pogge von Strandmann et al., 2017), but

620 slightly higher than that reported from solid phases of the altered oceanic crust (α = 0.985)
621 (Chan et al., 1992). It is also slightly higher than values reported for experimental or
622 theoretical uptake onto octahedral sites in clays (~0.98) (Dupuis et al., 2017; Hindshaw et
623 al., 2019), but in our case the fractionation factor also includes the effect of Li removal to
624 exchangeable and oxyhydroxide sites, and hence the α value is expected to be somewhat
625 higher (Pogge von Strandmann et al., 2020). We also note that Rayleigh-derived alpha
626 values will yield lower values than those from equilibrium fractionation.
627 Similarly, in our experiments from the present study, all samples show a negative co-
628 variation between δ^7Li values and Li/Na ratios (Fig. 11). The HCl experiment shows a trend
629 towards slightly lower δ^7Li values and higher Li/Na ratios compared to the starting solution,
630 which corresponds to Li addition from basalt dissolution. In contrast, the trends towards
631 higher δ^7Li and lower Li/Na in all the organic acid experiments document Li loss into
632 secondary minerals. For all experiments, the r^2 is slightly higher when the data are fit using a
633 logarithmic (r^2 = 0.85–0.98) rather than a linear (equilibrium fractionation) equation, which
634 supports the use of a Rayleigh-type model for Li removal, consistent with the closed-system
635 nature of the experiments. Thus, the best-fit α values for the organic acid experiments are
636 similar to those of the water-rock experiments: glycine: 0.991 ± 0.003; malic: 0.988 ± 0.004;
637 humic: 0987 ± 0.005; cinnamic: 0.984 ± 0.007. Overall, these fractionation factors are all
638 within error of each other, although the trend of the cinnamic acid experiment does appear
639 slightly different from the other experiments (Fig. 11). As detailed above, all the organic acid
640 and water experiments plot within the hematite stability field, and other likely precipitating
641 minerals include other Fe-oxyhydroxides, Ca- and Mg-smectites, kaolinite, and gibbsite,
642 which differ between experiments (Fig. 7). Given that clays dominate over oxyhydroxides in
643 the solid phase mass balance of the Li removed from solution (Fig. 8 and 9), the consistency

644 in the fractionation factors between experiments appears to suggest that different
645 secondary clay minerals impose similar fractionation factors during neoformation
646 (Hindshaw et al., 2019).

647 Importantly, the consistency in the fractionation factors also suggests that the
648 addition of organic acids does not change the Li isotope fractionation factor, but simply
649 drives the rate at which Li removal (with a constant fractionation factor) occurs, likely
650 because of changing secondary mineral formation rates. This scenario can readily explain
651 the different solution δ^7Li values (accompanied by different Li concentrations) in the
652 different experiments at the same timesteps (Fig. 3). It would also explain why fractionation
653 factors determined from the inorganic basaltic water-rock experiments (Pogge von
654 Strandmann et al., 2019b), and those inferred from relatively vegetation-poor basaltic
655 weathering environments such as Iceland (Pogge von Strandmann et al., 2006; Vigier et al.,
656 2009), are similar to those observed in highly vegetated basaltic environments such as the
657 Azores (Pogge von Strandmann et al., 2010) or Hawaii (Li et al., 2020). A corollary of the
658 similar fractionation factors observed in these experiments and in basaltic rivers (Liu et al.,
659 2015; Pogge von Strandmann et al., 2017; Pogge von Strandmann et al., 2010; Pogge von
660 Strandmann et al., 2006; Pogge von Strandmann et al., 2012; Pogge von Strandmann et al.,
661 2016; Vigier et al., 2009) is that even though plants have been observed to fractionate Li
662 isotopes (Li and Liu, 2020), they apparently have no discernible fractionation effect on river
663 waters. Therefore, we suggest that Li isotope changes in the Phanerozoic seawater record
664 (Kalderon-Asael et al., 2021) could be used to assess the indirect influence of plants on
665 inorganic weathering fluxes and congruence, rather than any specific effect of plant-
666 mediated weathering on the Li isotopic fractionation.
667

5.0 Conclusions

The addition of organic acids (glycine, malic acid, cinnamic acid, and humic acid), as well as a mineral acid (HCl), to basalt-water weathering experiments affected the pH and the behaviour of major and trace element concentrations, in part due to organic complexation with elements such as Mg and Fe.

In contrast to the behaviour of most elements, the different organic acids led to rather similar behaviour of Li concentrations and isotopes. In all cases, a mass balance of the reacted solids suggests that the Li lost from solution was predominantly taken up by clays (or amorphous clay-like precursors), with a more minor role for oxides/oxyhydroxides and then the exchangeable fraction. To a first order, the relative proportion of Li in these phases appears to have been controlled by pH, which indicates a potential route by which organic acids can influence Li partitioning during weathering.

The rates of Li removal into secondary clays were reduced by the presence of organic acids, but this process was still the major control on the Li isotope evolution. Final isotope fractionation between the exchangeable fraction and solution was $\Delta^7Li_{exch\text{-}soln}$ = -12.7 ± 1.7‰ for the organic experiments, compared to -11.8‰ for the inorganic water-rock experiments. In oxides, these values were $\Delta^7Li_{ox\text{-}soln}$ = -26.7 ± 0.4‰ for the organic acid experiments (-27.8‰ for inorganic water-rock experiments), and in clays they were $\Delta^7Li_{clay\text{-}soln}$ = -22.4 ± 1.7‰ (compared to -23.2‰ for inorganic water-rock experiments). Therefore, oxides exhibit the greatest magnitude of Li isotope fractionation, and the exchangeable fraction the least, but there is no resolvable effect due to the addition of organic acids. Solution δ^7Li values follow virtually the same negative trend of δ^7Li values versus Li/Na ratios for all the experiments, strongly suggesting that the combination of the exchangeable, oxide and clays phases combined impose similar bulk fractionation factors.

Since mineral saturation calculations suggest that different clay minerals would have formed in the different experiments, it appears that the Li isotope fractionation factors imposed by different clay minerals during clay neoformation are close to identical.

In these experiments, while organic acids: affect the behaviour of elements in solution; change the pH; reduce rates of secondary mineral formation; and slightly alter the Li partitioning between different secondary phases, they do not significantly alter Li isotope behaviour compared to inorganic experiments. As such, the recently reported increase in seawater δ^7Li values during the mid-Palaeozoic, which was at least partly attributed to terrestrialisation, does not appear to reflect a fundamental change in Li isotope behaviour, such as the effect of organic acids on Li isotope fractionation factors. Instead, changes in seawater δ^7Li values may be taken to indicate changes in weathering flux or congruence, allowing the effect of plant-mediated weathering on the carbon cycle to be assessed.

Acknowledgments:

The initial experiments were funded by Royal Society grant 537708. PPvS, DJW, AJK and GT were funded by ERC Consolidator grant 682760 CONTROLPASTCO2. DJW is currently supported by a NERC independent research fellowship (NE/T011440/1). Two anonymous reviewers are thanked for their constructive comments.

Adeleke R., Nwangburuka C. and Oboirien B. (2017) Origins, roles and fate of organic acids in soils: A review. *South African Journal of Botany* **108**, 393–406.

Algeo T. J. and Scheckler S. E. (1998) Terrestrial-marine teleconnections in the Devonian: links between the evolution of land plants, weathering processes, and marine anoxic events. *Philosophical Transactions of the Royal Society of London. Series B: Biological Sciences* **353**, 113-130.

Algeo T. J. and Scheckler S. E. (2010) Land Plant Evolution and Weathering Rate Changes in the Devonian. *Journal of Earth Sciences* **21**.

Andrews E., Pogge von Strandmann P. A. E. and Fantle M. S. (2020) Exploring the importance of authigenic clay formation in the global Li cycle. *Geochim. Cosmochim. Acta* **289**, 47–68.

Beerling D. J. and Berner R. A. (2005) Feedbacks and the coevolution of plants and atmospheric CO2. *Proceedings of the National Academy of Sciences* **102**, 1302-1305.

Berner E. K., Berner R. A. and Moulton K. L. (2003) 5.06 - Plants and Mineral Weathering: Present and Past. In *Treatise on Geochemistry* (eds. H. D. Holland and K. K. Turekian). Pergamon, Oxford. pp. 169-188.

Berner R. A. (1998) The carbon cycle and carbon dioxide over Phanerozoic time: the role of land plants. *Philosophical Transactions of the Royal Society of London B Biological Sciences* **353**, 75–82.

Berner R. A. (2006) GEOCARBSULF: A combined model for Phanerozoic atmospheric O2 and CO2. *Geochim. Cosmochim. Acta* **70**, 5653–5664.

Berner R. A., Lasaga A. C. and Garrels R. M. (1983) The Carbonate-Silicate Geochemical Cycle and Its Effect on Atmospheric Carbon-Dioxide over the Past 100 Million Years. *Am. J. Sci.* **283**, 641-683.

Brady P. V. and Walther J. V. (1989) Controls on silicate dissolution rates in neutral and basic pH solutions at 25°C. *Geochim. Cosmochim. Acta* **53**, 2823–2830.

Chan L. H. and Hein J. R. (2007) Lithium contents and isotopic compositions of ferromanganese deposites from the global ocean. *Deep-Sea Research* **54**, 1147-1162.

Chan L. H., Edmond J. M., Thompson G. and Gillis K. (1992) Lithium isotopic composition of submarine basalts: implications for the lithium cycle in the oceans. *Earth Planet. Sci. Lett.* **108**, 151-160.

Chemtob S. M., Rossman G. R. and Stebbins J. F. (2012) Natural hydrous amorphous silica: Quantitation of network speciation and hydroxyl content by 29Si MAS NMR and vibrational spectroscopy. *American Mineralogist* **97**, 203–211.

Clergue C., Dellinger M., Buss H. L., Gaillardet J., Benedetti M. F. and Dessert C. (2015) Influence of atmospheric deposits and secondary minerals on Li isotopes budget in a highly weathered catchment, Guadeloupe (Lesser Antilles). *Chem. Geol.* **414**, 28–41.

Dahl T. W. and Arens S. K. M. (2020) The impacts of land plant evolution on Earth's climate and oxygenation state – An interdisciplinary review. *Chem. Geol.* **547**, 119665.

Dellinger M., Gaillardet J., Bouchez J., Calmels D., Louvat P., Dosseto A., Gorge C., Alanoca L. and Maurice L. (2015) Riverine Li isotope fractionation in the Amazon River basin controlled by the weathering regimes. *Geochim. Cosmochim. Acta* **164**, 71–93.

Dontsova K., Balogh‐Brunstad Z. and Chorover J. (2020) Plants as Drivers of Rock Weathering. *Biogeochemical Cycles: Ecological Drivers and Environmental Impact*, 33-58.

Dontsova K., Zaharescu D., Henderson W., Verghese S., Perdrial N., Hunt E. and Chorover J. (2014) Impact of organic carbon on weathering and chemical denudation of granular basalt. *Geochim. Cosmochim. Acta* **139**, 508–526.

Dupuis R., Benoit M., Tuckerman M. E. and Méheut M. (2017) Importance of a fully anharmonic treatment of equilibrium isotope fractionation properties of dissolved ionic species as evidenced by Li+(aq). *Acconts of Chemical Research* **50**, 1597–1605.

Elliott T., Thomas A., Jeffcoate A. and Niu Y. L. (2006) Lithium isotope evidence for subduction-enriched mantle in the source of mid-ocean-ridge basalts. *Nature* **443**, 565–568.

765 Ganor J., Reznik I. J. and Roserberg Y. O. (2009) Organics in water-rock interactions. *Reviews*
766 *in Mineralogy and Geochemistry* **70**, 259–369.
767 Gibling M. R. and Davies N. S. (2012) Palaeozoic landscapes shaped by plant evolution.
768 *Nature Geoscience* **5**, 99–105.
769 Gíslason S. R., Arnorsson S. and Armannsson H. (1996) Chemical weathering of basalt in
770 southwest Iceland: Effects of runoff, age of rocks and vegetative/glacial cover. *Am. J.*
771 *Sci.* **296**, 837–907.
772 Golubev S. V., Bauer A. and Pokrovsky O. S. (2006) Effect of pH and organic ligands on the
773 kinetics of smectite dissolution at 25°C. *Geochim. Cosmochim. Acta* **70**, 4436–4451.
774 Gudbrandsson S., Wolff-Boenisch D., Gislason S. R. and Oelkers E. H. (2014) Experimental
775 determination of plagioclase dissolution rates as a function of its composition and
776 pH at 22 °C. *Geochim. Cosmochim. Acta* **139**, 154–172.
777 Heimburger A., Tharaud M., Monna F., Losno R., Desboeufs K. and Nguyen E. B. (2013) SLRS-
778 5 Elemental Concentrations of Thirty-Three Uncertified Elements Deduced from
779 SLRS-5/SLRS-4 Ratios. *Geostandards and Geoanalytical Research* **37**, 77-85.
780 Hindshaw R. S., Aciego S. M. and Tipper E. T. (2018) Li and U Isotopes as a Potential Tool for
781 Monitoring Active Layer Deepening in Permafrost Dominated Catchments. *Frontiers*
782 *in Earth Science* **6**.
783 Hindshaw R. S., Tosca R., Gout T. L., Farnan I., Tosca N. J. and Tipper E. T. (2019)
784 Experimental constraints on Li isotope fractionation during clay formation. *Geochim.*
785 *Cosmochim. Acta* **250**, 219–237.
786 Huh Y., Chan L. H. and Edmond J. M. (2001) Lithium isotopes as a probe of weathering
787 processes: Orinoco River. *Earth Planet. Sci. Lett.* **194**, 189–199.
788 Huh Y., Chan L. H., Zhang L. and Edmond J. M. (1998) Lithium and its isotopes in major world
789 rivers: Implications for weathering and the oceanic budget. *Geochim. Cosmochim.*
790 *Acta* **62**, 2039–2051.
791 Jackson T. A. (2015) Weathering, secondary mineral genesis, and soil formation caused by
792 lichens and mosses growing on granitic gneiss in a boreal forest environment.
793 *Geoderma* **251-252**, 78-91.
794 Jeffcoate A. B., Elliott T., Thomas A. and Bouman C. (2004) Precise, small sample size
795 determinations of lithium isotopic compositions of geological reference materials
796 and modern seawater by MC-ICP-MS. *Geostandards and Geoanalytical Research* **28**,
797 161-172.
798 Jiang X., Lin X., Yao D., Zhai S. and Guo W. (2007) Geochemistry of lithium in marine
799 ferromanganese oxide deposits. *Deep-Sea Research I* **54**, 85–98.
800 Jones D. L. (1998) Organic acids in the rhizosphere – a critical review. *Plant and Soil* **205**, 25–
801 44.
802 Jones M. T., Pearce C. R. and Oelkers E. H. (2012) An experimental study of the interaction
803 of basaltic riverine particulate material and seawater. *Geochim. Cosmochim. Acta* **77**,
804 108–120.
805 Kalderon-Asael B., Katchinoff J. A. R., Planavsky N. J., Hood A. v. S., Dellinger M., Bellefroid E.
806 J., Jones D. S., Hofmann A., Ossa Ossa F., Macdonald F. A., Wang C., Isson T. T.,
807 Murphy J. G., Higgins J. A., West A. J., Wallace M. W., Asael D. and Pogge von
808 Strandmann P. A. E. (2021) A lithium-isotope perspective on the evolution of carbon
809 and silicon cycles. *Nature* **595**, 394–398.

Kennedy M. J. and Wagner T. (2011) Clay mineral continental amplifier for marine carbon sequestration in a greenhouse ocean. *Proceedings of the National Academy of Sciences* **108**, 9776–9781.

Kenrick P. (2003) Palaeobotany - Fishing for the first plants. *Nature* **425**, 248-249.

Kenrick P., Wellman C. H., Schneider H. and Edgecombe G. D. (2012) A timeline for terrestrialization: consequences for the carbon cycle in the Palaeozoic. *Philosophical Transactions of the Royal Society of London B Biological Sciences* **367**, 519–536.

Kisakürek B., James R. H. and Harris N. B. W. (2005) Li and δ^7Li in Himalayan rivers: Proxies for silicate weathering? *Earth Planet. Sci. Lett.* **237**, 387–401.

Lalonde K., Mucci A., Ouellet A. and Gelinas Y. (2012) Preservation of organic matter in sediments promoted by iron. *Nature* **483**, 198–200.

Lemarchand E., Chabaux F., Vigier N., Millot R. and Pierret M. C. (2010) Lithium isotope systematics in a forested granitic catchment (Strengbach, Vosges Mountains, France). *Geochim. Cosmochim. Acta* **74**, 4612-4628.

Lenton T. M., Daines S. J. and Mills B. J. W. (2018) COPSE reloaded: An improved model of biogeochemical cycling over Phanerozoic time. *Earth-Science Reviews* **178**, 1–28.

Lenton T. M., Crouch M., Johson M., Pires N. and Dolan L. (2012) First plants cooled the Ordovician. *Nature Geoscience* **5**, 86–89.

Li W. and Liu X.-M. (2020) Experimental investigation of lithium isotope fractionation during kaolinite adsorption: Implications for chemical weathering. *Geochim. Cosmochim. Acta* **284**, 156–172.

Li W., Liu X.-M. and Chadwick O. A. (2020) Lithium isotope behavior in Hawaiian regoliths: Soil-atmosphere-biosphere exchanges. *Geochim. Cosmochim. Acta* **285**, 175–192.

Liu X.-M., Wanner C., Rudnick R. L. and McDonough W. F. (2015) Processes controlling δ7Li in rivers illuminated by study of streams and groundwaters draining basalts. *Earth Planet. Sci. Lett.* **409**, 212–224.

Ma T., Weynell M., Li S. L., Liu Y., Chetelat B., Zhong J., Xu S. and Liu C. Q. (2020) Lithium isotope compositions of the Yangtze River headwaters: Weathering in high-relief catchments. *Geochim. Cosmochim. Acta* **280**, 46–65.

Ma Z., Gray E., Thomas E., Murphy B., Zachos J. C. and Paytan A. (2014) Carbon sequestration during the Palaeocene– Eocene Thermal Maximum by an efficient biological pump. *Nature Geoscience* **7**, 382–388.

Merkel B. J. and Planer-Friedrich B. (2005) *Groundwater Geochemistry*. Springer.

Millot R., Scaillet B. and Sanjuan B. (2010) Lithium isotopes in island arc geothermal systems: Guadeloupe, Martinique (French West Indies) and experimental approach. *Geochim. Cosmochim. Acta* **74**, 1852-1871.

Murphy M. J., Porcelli D., Pogge von Strandmann P. A. E., Hirst C. A., Kutscher L., Katchinoff J. A., Mörth C.-M., Maximov T. and Andersson P. S. (2019) Tracing silicate weathering processes in the permafrost-dominated Lena River watershed using lithium isotopes. *Geochim. Cosmochim. Acta* **245**, 154–171.

Parkhurst D. L. and Appelo C. A. J. (1999) User's guide to PHREEQC (version 2) - a computer program for speciation, batch-reaction, one-dimensional transport, and inverse geochemical calculations, Water-Resouces Investigations.

Penniston-Dorland S., Liu X.-M. and Rudnick R. L. (2017) Lithium Isotope Geochemistry. In *Rev. Min. Geochem.* pp. 165–217.

Pistiner J. S. and Henderson G. M. (2003) Lithium-isotope fractionation during continental weathering processes. *Earth Planet. Sci. Lett.* **214**, 327-339.

857 Pogge von Strandmann P. A. E. and Henderson G. M. (2015) The Li isotope response to
858 mountain uplift. *Geology* **43**, 67–70.
859 Pogge von Strandmann P. A. E., Jenkyns H. C. and Woodfine R. G. (2013) Lithium isotope
860 evidence for enhanced weathering during Oceanic Anoxic Event 2. *Nature*
861 *Geoscience* **6**, 668–672.
862 Pogge von Strandmann P. A. E., Frings P. J. and Murphy M. J. (2017) Lithium isotope
863 behaviour during weathering in the Ganges Alluvial Plain. *Geochim. Cosmochim. Acta*
864 **198**, 17–31.
865 Pogge von Strandmann P. A. E., Kasemann S. A. and Wimpenny J. B. (2020) Lithium and
866 Lithium Isotopes in Earth's Surface Cycles. *Elements* **16**, 253–258.
867 Pogge von Strandmann P. A. E., Dellinger M. and West A. J. (2021a) *Lithium Isotopes: A*
868 *Tracer of Past and Present Silicate Weathering*. Cambridge University Press.
869 Pogge von Strandmann P. A. E., Burton K. W., James R. H., van Calsteren P. and Gislason S. R.
870 (2010) Assessing the role of climate on uranium and lithium isotope behaviour in
871 rivers draining a basaltic terrain. *Chem. Geol.* **270**, 227–239.
872 Pogge von Strandmann P. A. E., Burton K. W., James R. H., van Calsteren P., Gislason S. R.
873 and Mokadem F. (2006) Riverine behaviour of uranium and lithium isotopes in an
874 actively glaciated basaltic terrain. *Earth Planet. Sci. Lett.* **251**, 134–147.
875 Pogge von Strandmann P. A. E., Opfergelt S., Lai Y. J., Sigfusson B., Gislason S. R. and Burton
876 K. W. (2012) Lithium, magnesium and silicon isotope behaviour accompanying
877 weathering in a basaltic soil and pore water profile in Iceland. *Earth Planet. Sci. Lett.*
878 **339–340**, 11–23.
879 Pogge von Strandmann P. A. E., Schmidt D. N., Planavsky N. J., Wei G., Todd C. L. and
880 Baumann K.-H. (2019a) Assessing bulk carbonates as archives for seawater Li isotope
881 ratios. *Chem. Geol.* **530**, 119338.
882 Pogge von Strandmann P. A. E., Renforth P., West A. J., Murphy M. J., Luu T.-H. and
883 Henderson G. M. (2021b) The lithium and magnesium isotope signature of olivine
884 dissolution in soil experiments. *Chem. Geol.* **560**, 120008.
885 Pogge von Strandmann P. A. E., Elliott T., Marschall H. R., Coath C., Lai Y. J., Jeffcoate A. B.
886 and Ionov D. A. (2011) Variations of Li and Mg isotope ratios in bulk chondrites and
887 mantle xenoliths. *Geochim. Cosmochim. Acta* **75**, 5247–5268.
888 Pogge von Strandmann P. A. E., Burton K. W., Opfergelt S., Eiriksdottir E. S., Murphy M. J.,
889 Einarsson A. and Gislason S. R. (2016) The effect of hydrothermal spring weathering
890 processes and primary productivity on lithium isotopes: Lake Myvatn, Iceland. *Chem.*
891 *Geol.* **445**, 4–13.
892 Pogge von Strandmann P. A. E., Fraser W. T., Hammond S. J., Tarbuck G., Wood I. G., Oelkers
893 E. H. and Murphy M. J. (2019b) Experimental determination of Li isotope behaviour
894 during basalt weathering. *Chem. Geol.* **517**, 34–43.
895 Pogge von Strandmann P. A. E., Porcelli D., James R. H., van Calsteren P., Schaefer B. F.,
896 Cartwright I., Reynolds B. C. and Burton K. W. (2014) Chemical weathering processes
897 in the Great Artesian Basin: Evidence from lithium and silicon isotopes. *Earth Planet.*
898 *Sci. Lett.* **406**, 24–36.
899 Poulton S. W. and Canfield D. E. (2005) Development of a sequential extraction procedure
900 for iron: implications for iron partitioning in continentally derived particulates.
901 *Chem. Geol.* **214**, 209–221.

902 Richter F. M., Davis A. M., DePaolo D. J. and Watson E. B. (2003) Isotope fractionation by
903 chemical diffusion between molten basalt and rhyolite. *Geochim. Cosmochim. Acta*
904 **67**, 3905-3923.
905 Richter F. M., Mendybaev R. A., Christensen J. N., Hutcheon I. D., Williams R. W., Sturchio N.
906 C. and Belsos Jr. A. D. (2006) Kinetic isotopic fractionation during diffusion of ionic
907 species in water. *Geochim. Cosmochim. Acta* **70**, 277-289.
908 Sauzéat L., Rudnick R. L., Chauvel C., Garcon M. and Tang M. (2015) New perspectives on
909 the Li isotopic composition of the upper continental crust and its weathering
910 signature. *Earth Planet. Sci. Lett.* **428**, 181–192.
911 Sonntag I. (2007) Distribution of Lithium, Beryllium and Boron in Phenocrysts of calc-alkaline
912 Rocks from Nisyros (Aegean Sea). PhD Heidelberg.
913 Sposito G. (2008) *The Chemistry of Soils*. Oxford University Press.
914 Stefansdottir M. B. and Gislason S. R. (2005) The erosion and suspended matter/seawater
915 interaction during and after the 1996 outburst flood from the Vatnajokull Glacier,
916 Iceland. *Earth Planet. Sci. Lett.* **237**, 433-452.
917 Stefansson A. and Gislason S. R. (2001) Chemical weathering of basalts, Southwest Iceland:
918 Effect of rock crystallinity and secondary minerals on chemical fluxes to the ocean.
919 *Am. J. Sci.* **301**, 513-556.
920 Steinhoefel G., Brantley S. L. and Fantle M. S. (2021) Lithium isotopic fractionation during
921 weathering and erosion of shale. *Geochim. Cosmochim. Acta* **295**, 155–177.
922 Tessier A., Campbell P. G. C. and Bisson M. (1979) Sequential Extraction Procedure for the
923 Speciation of Particulate Trace Metals. *Analytical Chemistry* **51**, 844-851.
924 Tipper E. T., Stevenson E. I., Alcock V., Knight A. C. G., Baronas J. J., Hilton R. G., Bickle M. J.,
925 Larkin C. S., Feng L., Relph K. E. and Hughes G. (2021) Global silicate weathering flux
926 overestimated because of sediment–water cation exchange. *Proceedings of the*
927 *National Academy of Sciences* **118**, e2016430118.
928 Tomascak P. B., Magna T. and Dohmen R. (2016) *Advances in Lithium Isotope Geochemistry*.
929 Springer.
930 Tsai P.-H., You C.-F., Huang K.-F., Chung C.-H. and Sun Y.-B. (2014) Lithium distribution and
931 isotopic fractionation during chemical weathering and soil formation in a loess
932 profile. *Journal of Asian Earth Sciences* **87**, 1–10.
933 Uysal N., Kizildag S., Yuce Z., Guvendi G., Kandis S., Koc B., Karakilic A., Camsari U. M. and
934 Ates M. (2018) Timeline (Bioavailability) of Magnesium Compounds in Hours: Which
935 Magnesium Compound Works Best? *Biological Trace Element Research*
936 10.1007/s12011-018-1351-9.
937 Valle N., Verney-Carron A., Sterpenich J., Libourel G., Deloule E. and Jollivet P. (2010)
938 Elemental and isotopic (29Si and 18O) tracing of glass alteration mechanisms.
939 *Geochim. Cosmochim. Acta* **74**, 3412–3431.
940 Verney-Carron A., Vigier N. and Millot R. (2011) Experimental determination of the role of
941 diffusion on Li isotope fractionation during basaltic glass weathering. *Geochim.*
942 *Cosmochim. Acta* **75**, 3452–3468.
943 Vigier N., Gislason S. R., Burton K. W., Millot R. and Mokadem F. (2009) The relationship
944 between riverine lithium isotope composition and silicate weathering rates in
945 Iceland. *Earth Planet. Sci. Lett.* **287**, 434–441.
946 Vigier N., Decarreau A., Millot R., Carignan J., Petit S. and France-Lanord C. (2008)
947 Quantifying Li isotope fractionation during smectite formation and implications for
948 the Li cycle. *Geochim. Cosmochim. Acta* **72**, 780–792.

Walker J. C. G., Hays P. B. and Kasting J. F. (1981) A Negative Feedback Mechanism for the Long-Term Stabilization of Earths Surface-Temperature. *Journal of Geophysical Research-Oceans and Atmospheres* **86**, 9776-9782.

Wang X., Li Q., Hu H., Zhang T. and Zhou Y. (2005) Dissolution of kaolinite induced by citric, oxalic, and malic acids. *Journal of Colloid and Interface Science* **290**, 481–488.

Welch S. A. and Ullman W. J. (1993) The effect or organic acids on plagioclase dissolution rates and stoichiometry. *Geochim. Cosmochim. Acta* **57**, 2725-2736.

Wilson D. J., Piotrowski A. M., Galy A. and Clegg J. A. (2013) Reactivity of neodymium carriers in deep sea sediments: Implications for boundary exchange and paleoceanography. *Geochim. Cosmochim. Acta* **109**, 197–221.

Wimpenny J., James R. H., Burton K. W., Gannoun A., Mokadem F. and Gislason S. R. (2010a) Glacial effects on weathering processes: New insights from the elemental and lithium isotopic composition of West Greenland rivers *Earth Planet. Sci. Lett.* **290**, 427-437.

Wimpenny J., Gislason S. R., James R. H., Gannoun A., Pogge von Strandmann P. A. E. and Burton K. W. (2010b) The behaviour of Li and Mg isotopes during primary phase dissolution and secondary mineral formation in basalt. *Geochim. Cosmochim. Acta* **74**, 5259-5279.

Wimpenny J., Colla C. A., Yu P., Yin Q. Z., Rustad J. R. and Casey W. H. (2015) Lithium isotope fractionation during uptake by gibbsite. *Geochim. Cosmochim. Acta* **168**, 133–150.

Zhang L., Chan L.-H. and Gieskes J. M. (1998) Lithium isotope geochemistry of pore waters from ocean drilling program Sites 918 and 919, Irminger Basin. *Geochim. Cosmochim. Acta* **62**, 2437-2450.

Experiment	Sample	Time	pH	Na	Mg	Al	Si	K	Ca	Fe	Li	δ^7Li	2sd
		days		mg/L	mg/L	µg/L	mg/L	mg/L	mg/L	µg/L	µg/L	‰	
	Initial water	0	6.84	48.5	7.87	b.d.l.	2.59	11.1	11.8	5.4	13.5	14.7	0.4
Glycine	1.1	1	7.40	49.9	9.52	3.00	3.02	10.1	12.0	7.3	10.5	15.6	0.2
	1.2	2	7.41	50.0	10.0	3.63	3.22	10.0	11.8	8.5	9.89	15.5	0.2
	1.3	4	7.45	50.9	10.7	6.19	3.60	9.91	12.2	7.0	8.46	17.9	0.1
	1.4	12	7.30	50.4	11.5	2.21	4.64	10.9	14.9	1.1	5.34		
	1.5	34	7.00	51.8	12.3	b.d.l.	5.78	12.5	11.5	b.d.l.	4.03	27.3	0.3
	1.6	68	7.12	52.1	12.5	4.20	5.93	12.4	11.2	14.7	3.51	31.5	0.3
	1.7	126	7.12	51.8	12.7	1.34	6.09	12.1	11.8	b.d.l.	2.55	30.8	0.3
	1.8	252	7.79	51.8	14.2	3.65	9.95	11.0	12.8	7.2	3.04	29.3	0.2
Malic acid	5.1	1	3.29	50.7	10.4	4350	7.29	10.7	12.6	2690	12.3	15.9	0.1
	5.2	2	3.41	51.8	13.2	13800	14.4	10.6	13.1	12500	12.1	14.5	0.4
	5.3	4	3.55	54.1	20.0	14900	25.2	10.8	14.2	27600	13.0	14.7	0.4
	5.4	12	4.04	54.6	37.6	4700	13.5	10.2	14.2	8860	13.8	14.4	0.2
	5.5	34	5.83	54.1	46.7	20600	31.1	8.88	14.6	54500	10.8	18.2	0.2
	5.6	68	6.63	54.7	45.9	3260	9.12	8.68	12.9	8580	7.25	24.1	0.1
	5.7	126	6.44	54.4	46.8	58.9	17.1	8.87	6.6	42.1	3.67	35.5	0.3
	5.8	252	6.93	53.9	47.1	12.1	14.0	8.62	8.8	3.9	2.96	34.9	0.1
Cinnamic acid	9.1	1	4.95	47.9	9.11	14.3	3.09	10.0	12.2	5.5	11.4	15.9	0.4
	9.2	2	4.90	48.5	10.5	46.6	3.86	9.90	12.2	11.5	10.7	15.7	0.2
	9.3	4	4.90	48.1	11.4	88.9	5.41	9.71	12.3	15.2	10.0	16.2	0.1
	9.4	12	4.96	48.4	12.1	41.5	8.62	9.71	12.7	5.9	9.24	20.2	0.4
	9.5	34	4.96	48.3	12.6	33.9	13.2	9.73	12.9	16.3	8.25	26.1	0.4
	9.6	68	5.35	48.5	12.9	18.8	16.0	9.57	12.8	4.9	7.09	29.3	0.2
	9.7	126	5.12	48.8	13.1	13.2	19.5	9.37	12.8	8.0	5.24	28.3	0.3
	9.8	252	4.77	49.2	13.7	58.1	23.1	9.57	13.3	22.1	4.63	31.0	0.2
HCl	11.1	1	2.26	50.6	11.0	2030	5.05	11.0	13.2	446	12.6	13.3	0.4
	11.2	2	2.47	51.4	14.7	7580	11.5	11.6	14.9	1280	13.2	14.3	0.4
	11.3	4	3.06	52.3	19.3	2300	27.8	12.0	16.4	5030	14.7	13.8	0.4
	11.4	12	3.58	52.8	20.5	26800	37.1	11.8	16.9	1650	15.3	12.7	0.2
	11.5	34	3.66	52.5	21.5	26700	43.7	11.8	17.2	1900	16.4	11.8	0.2
	11.6	68	4.03	52.3	21.7	25700	45.9	11.6	17.3	3690	16.6	13.1	0.1
	11.7	126	3.80	53.5	22.3	25100	48.1	11.7	17.9	218	17.2	12.5	0.2
	11.8	252	3.31	54.1	23.0	23300	49.1	11.6	18.2	117	17.3	12.8	0.4
Humic acid	13.1	1	4.58	47.3	9.05	164	3.52	10.1	10.8	10.8	11.9	15.0	0.1
	13.2	2	4.46	48.1	10.0	123	4.28	10.2	10.6	11.0	11.9	14.1	0.2
	13.3	4	4.82	47.7	10.4	118	4.88	9.87	10.2	13.5	11.1	14.4	0.4
	13.4	12	5.04	47.0	11.2	24.2	6.77	9.51	10.5	6.8	9.56	16.5	0.2
	13.5	34	5.32	47.7	12.2	12.1	9.57	9.58	10.6	5.3	7.61	21.7	0.5
	13.6	68	5.34	47.1	12.3	4.11	11.2	9.35	10.4	4.7	5.92	23.9	0.4
	13.7	126	5.22	47.3	12.4	2.23	13.0	9.34	10.1	3.7	3.92	29.5	0.1
	13.8	252	5.06	47.4	12.6	7.71	14.0	9.03	10.1	5.4	2.78	32.7	0.1
Water	15.1	1	6.91	47.8	9.28	8.50	3.19	9.63	11.9	10.5	9.87	15.8	0.1
	15.2	2	6.86	48.4	9.92	5.58	3.41	9.32	11.5	6.3	9.89	16.8	0.3
	15.3	4	6.89	48.4	10.6	8.65	3.61	8.95	11.0	7.3	8.22	19.6	0.2
	15.4	12	7.17	48.6	10.9	11.7	4.22	8.67	10.8	8.4	4.68	26.2	0.3
	15.5	34	7.60	48.8	11.2	10.7	4.83	8.56	10.6	6.7	2.86	31.0	0.2
	15.6	68	7.33	48.9	11.2	10.7	5.20	8.46	10.6	6.4	2.20	32.7	0.4
	15.7	126	7.08	48.7	11.4	12.3	5.71	8.35	10.8	6.7	1.60	34.4	0.3
	15.8	252	7.04	49.4	11.5	11.7	6.18	8.35	10.8	7.7	1.31	33.3	0.3
Water	16.1	1	7.26								9.5	15.4	0.3
	16.2	2	7.05								9.5	16.0	0.3
	16.3	4	7.13								8.0	19.6	0.2
	16.4	12	7.43								4.8	24.1	0.4
	16.5	34	7.49								2.8	31.5	0.1
	16.6	68	7.29								2.3	33.2	0.1
	16.7	126	7.16								1.4	34.9	0.3
	16.8	252	7.31								1.4	33.3	0.4

978

979 Table 1. Solution elemental concentration and Li isotope data for the different experiments.

980 The water-rock experimental data are from Pogge von Strandmann et al. (2019).

981 b.d.l., below detection limit

982

Phase	Sample	δ^{7}Li ‰	2sd	Total Li ug	Mg/Si g/g	Ca/Si g/g	K/Si g/g	Li/Si g/g	Al/Si g/g	Fe/Si g/g
Exchangeable	Exp 1 (glycine)	20.8	0.4	2.08	9.23	79.2	8.5	0.035	0.18	0.04
	Exp 5 (malic)	21.6	0.3	2.28	10.7	44.5	4.6	0.012	0.18	0.03
	Exp 9 (cinnamic)	16.8	0.2	2.46	10.1	109	15.4	0.067	0.17	0.03
	Exp 11 (HCl)	2.6	0.3	0.69	6.44	56.10	7.84	0.011	0.18	0.03
	Exp 13 (humic)	17.9	0.6	2.58	8.76	94.2	8.4	0.028	0.21	0.05
	Exp 15 (water)	21.3	0.4	2.47	9.47	113	12.6	0.030	0.21	0.03
	Exp 16 (water)	21.8	0.5	2.90	8.24	96.4	10.4	0.015	0.19	0.03
	Unreacted	17.8	0.1	1.32	25.3	104	9.3	0.038	0.18	0.03
Oxide	Exp 1 (glycine)	2.8	0.2	3.91	3.42	6.22	0.0867	0.00044	9.66	8.22
	Exp 5 (malic)	8.0	0.7	3.42	3.11	6.20	0.0882	0.00052	9.32	8.76
	Exp 9 (cinnamic)	3.8	0.3	2.11	3.61	6.57	0.0931	0.00056	9.20	9.05
	Exp 11 (HCl)	-4.0	0.2	1.91	3.44	6.11	0.0782	0.00028	4.21	5.88
	Exp 13 (humic)	6.5	0.3	2.60	3.71	6.38	0.0925	0.00047	10.6	10.7
	rpt	6.1	0.3							
	Exp 15 (water)	5.5	0.0	3.93	3.57	6.42	0.0913	0.00048	9.17	8.43
	Exp 16 (water)	5.5	0.3	3.41	3.61	6.46	0.0898	0.00046	8.96	8.58
	Unreacted	3.7	0.4	1.49	3.53	6.40	0.0902	0.00050	8.49	7.97
Sec. mins.	Exp 1 (glycine)	8.6	0.5	25.2	0.306	0.422	0.013	0.0005	0.594	0.895
	rpt	8.4	0.3							
	Exp 5 (malic)	10.0	0.2	25.7	0.377	0.481	0.022	0.0005	0.814	1.09
	Exp 9 (cinnamic)	8.8	0.2	25.5	0.306	0.458	0.013	0.0004	0.594	0.873
	Exp 11 (HCl)	4.8	0.1	17.9	0.297	0.415	0.013	0.0001	0.625	0.928
	Exp 13 (humic)	10.7	0.4	26.7	0.311	0.433	0.015	0.0006	0.756	0.984
	rpt	10.2	0.2							
	Exp 15	9.3	0.6	27.5	0.271	0.439	0.014	0.0003	0.567	0.819
	Exp 16	10.8	0.1	27.0	0.292	0.426	0.013	0.0002	0.634	0.926
	Unreacted	5.3	0.5	17.6	0.294	0.426	0.013	0.0005	0.635	0.921
Bulk	Exp 1 (glycine)	3.8	0.1	1370						
	rpt	4.1	0.4							
	Exp 5 (malic)	3.4	0.1	1410						
	rpt	3.7	0.5							
	Exp 9 (cinnamic)	3.7	0.2	1370						
	Exp 11 (HCl)	3.4	0.1	1350						
	Exp 13 (humic)	4.0	0.2	1380						
	Exp 15	4.5	0.2	1320						
	Exp 16	4.1	0.3	1390						
	Unreacted	4.4	0.2	1380	0.269	0.590	0.020	0.00003	0.358	0.531

Table 2. Elemental ratios, Li amounts (i.e. Li concentration normalised to leached mass), and Li isotope values from the sequential leaches of the unreacted basalt and the reacted basalt from each experiment. The values for the water-rock experiments and the unreacted basalt are from Pogge von Strandmann et al. (2019). Repeats (rpt) are full procedural repeats, including leaching, chemistry and analysis.

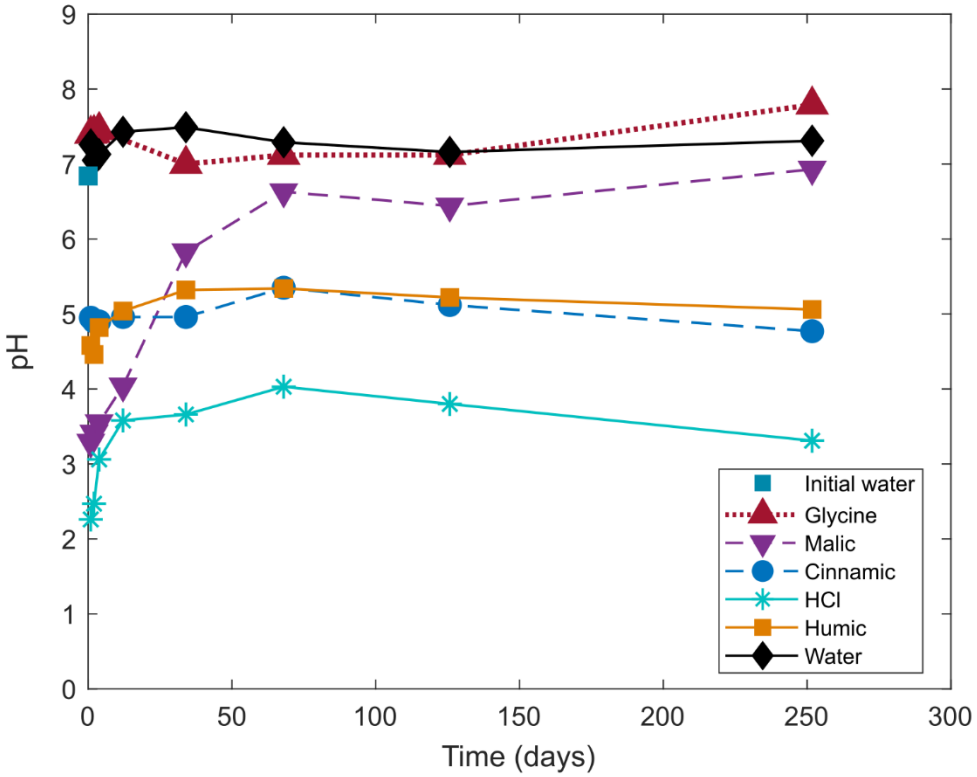

991

992 Figure 1. Solution pH with time for each experiment. The blue square represents the initial

993 unreacted water.

994

995

996

997

998

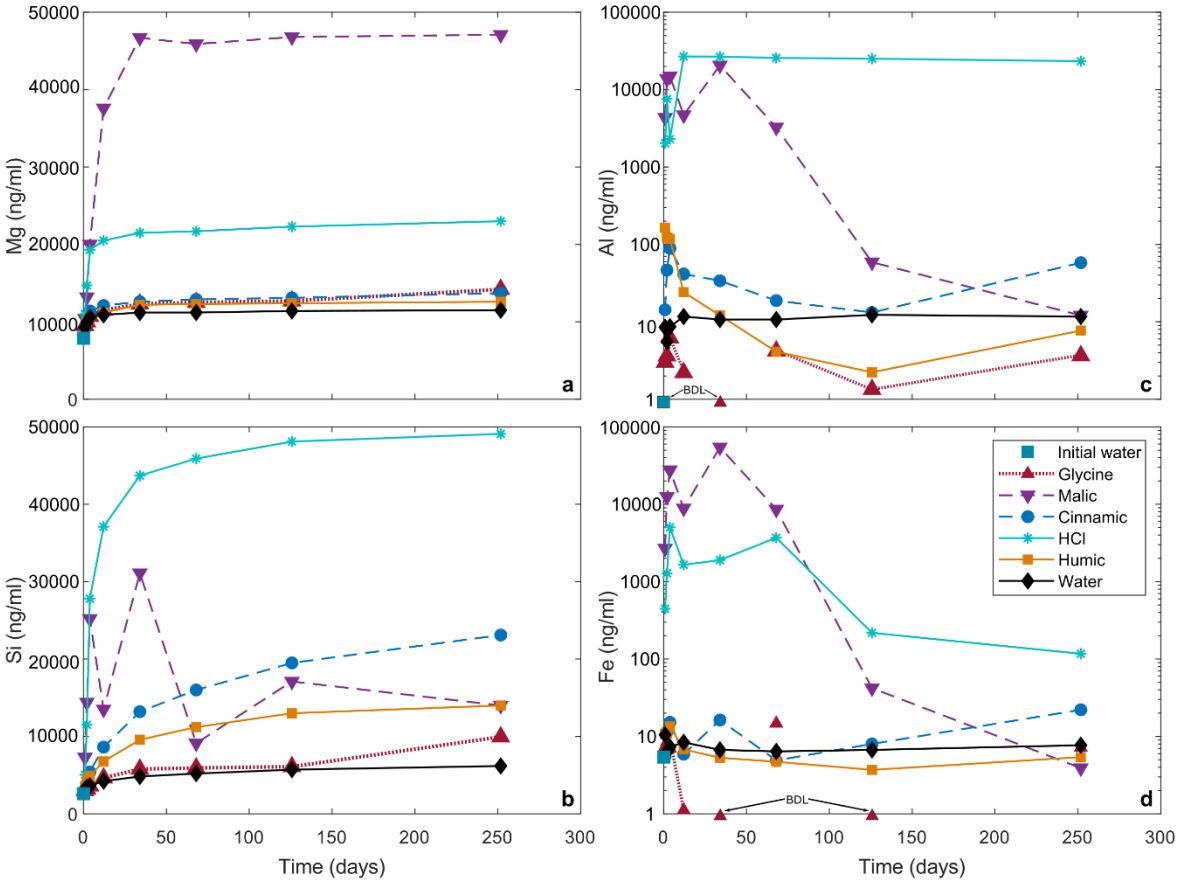

999

1000 Figure 2. Elemental concentrations with time for each experiment (a: Mg; b: Si; c: Al; d: Fe).

1001 The solid blue squares are the initial unreacted water. Note the logarithmic y-axis for panels

1002 c and d and that in c) the initial water and one of the glycine samples were below the

1003 detection limits (BDL), while in d) two of the glycine samples were BDL.

1004

1005

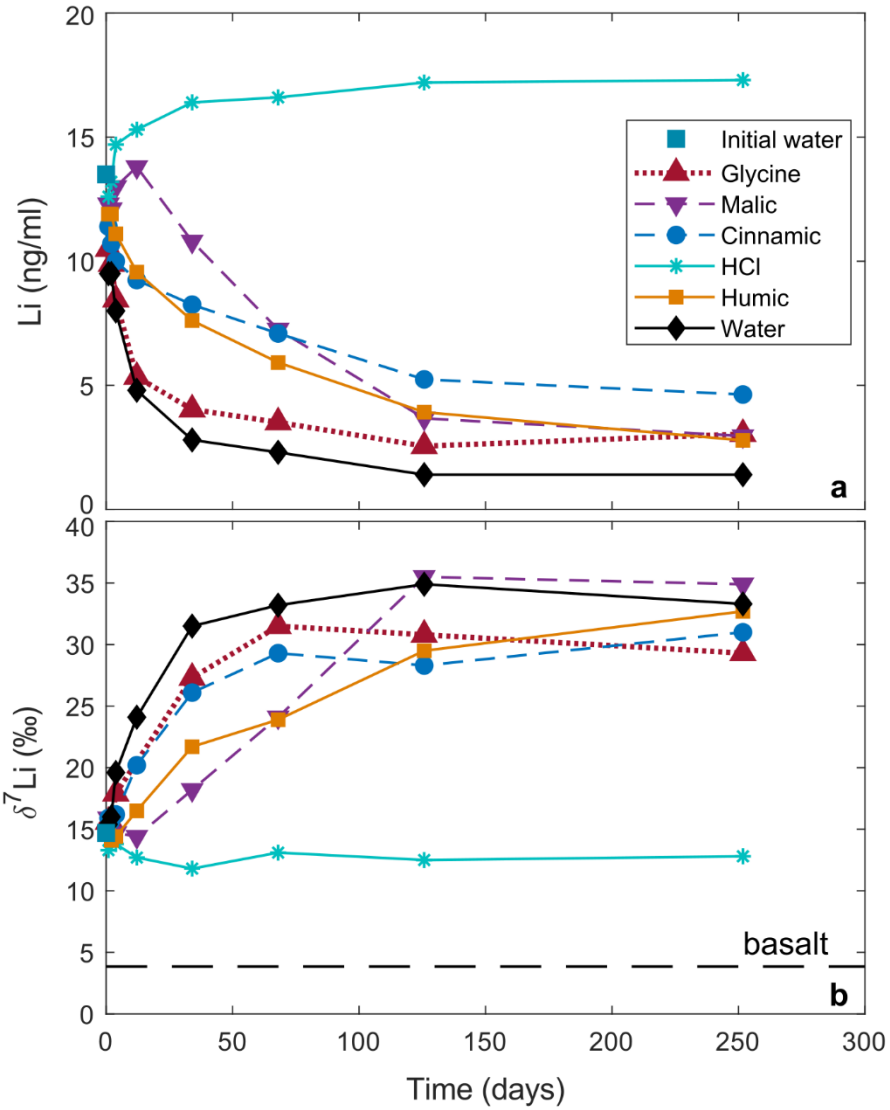

1006

1007 Figure 3. Temporal evolution of (a) solution Li concentrations and (b) Li isotope

1008 compositions for each experiment.

1009

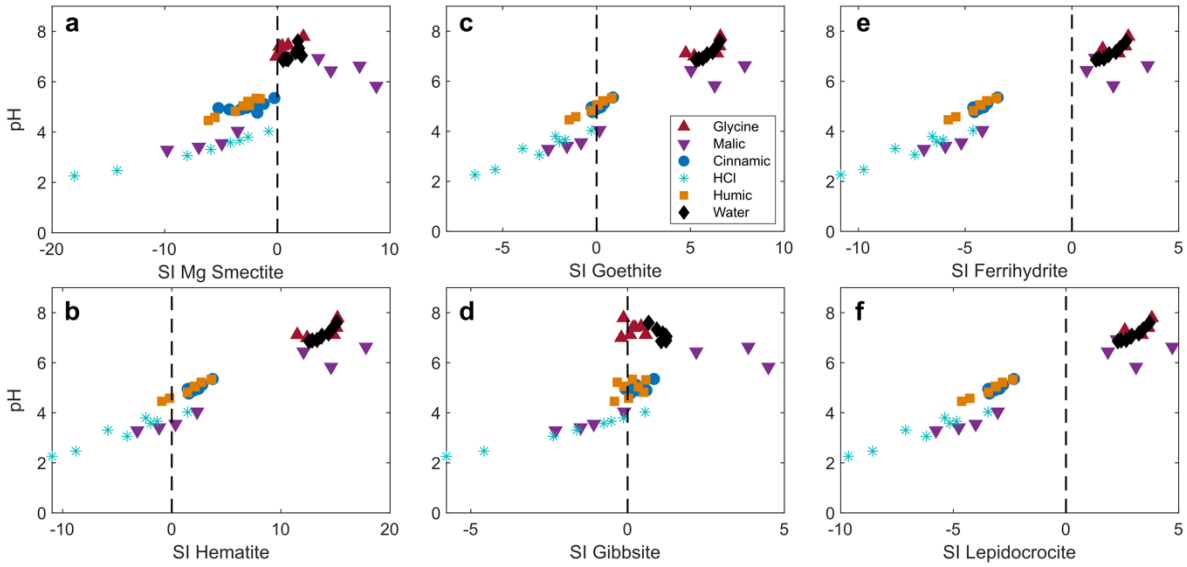

Figure 4. The saturation indices for (a) Mg-smectite, (b) hematite, (c) goethite, (d) gibbsite, (e) ferrihydrite, and (f) lepidocrocite for each experiment plotted against solution pH. The dashed vertical lines indicate saturation.

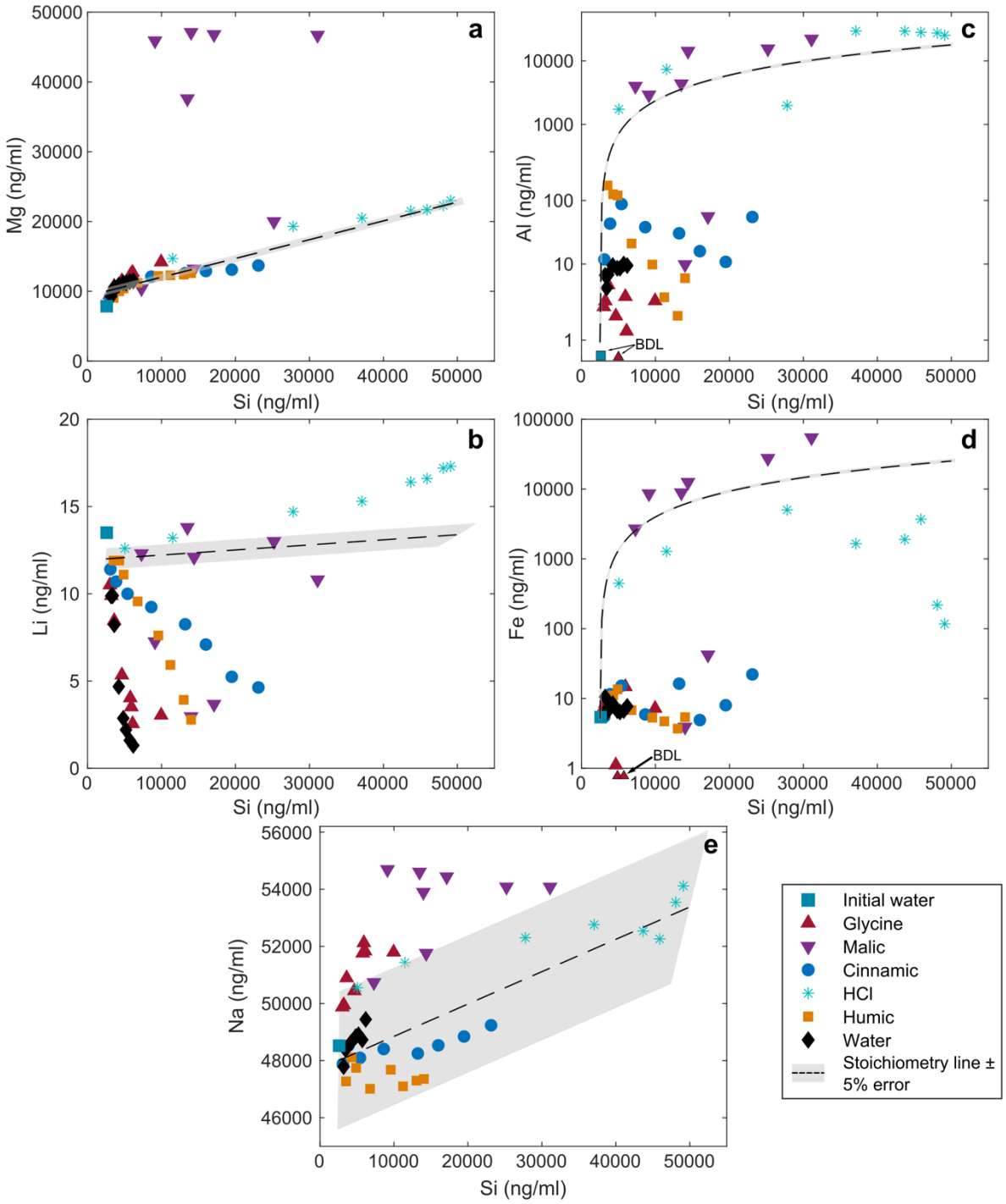

1020

1021 Figure 5. Assessment of dissolution stoichiometry for different elements as a function of Si

1022 concentrations: a) Mg, b) Li, c) Al, d) Fe, e) Na. The dashed black lines represent

1023 stoichiometric dissolution of the bulk basalt from the initial water composition. The error

1024 bands on these lines represent the analytical uncertainty, such that data points that plot

1025 within the bands are within uncertainty of stoichiometry. Note that panels c and d have a

1026 logarithmic y-axis and that in c) the initial water and one of the glycine samples were below
1027 the detection limits (BDL), while in d) two of the glycine samples were BDL.
1028
1029
1030
1031

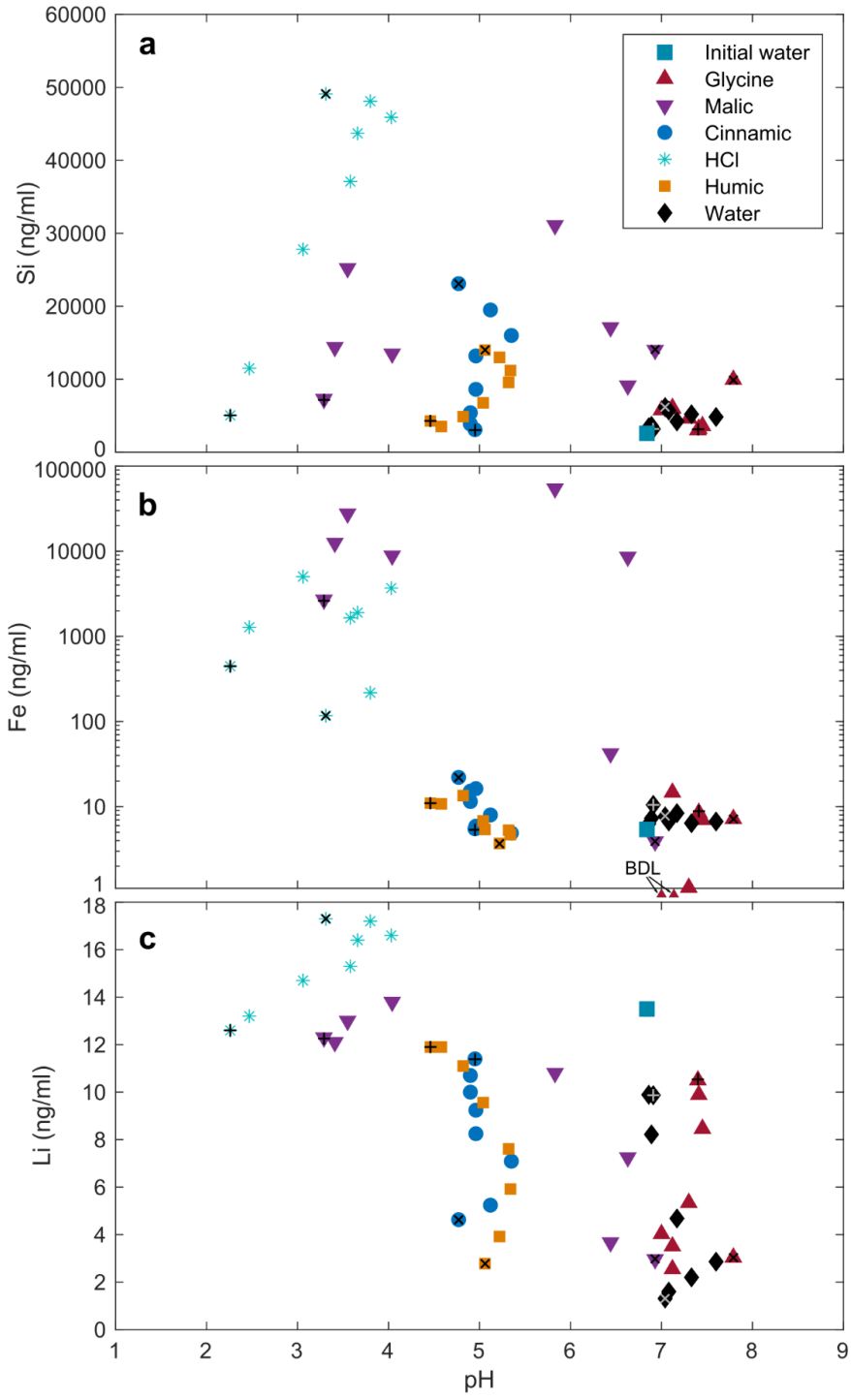

1032

1033 Figure 6. Elemental concentrations of (a) Si, (b) Fe and (c) Li as a function of solution pH for

1034 each experiment. Horizontal crosses within symbols (black for acids, grey for water) indicate

1035 the initial point of each experiment, while diagonal crosses (black for acids, grey for water)

1036 within symbols represent the final point of each experiment.

1037

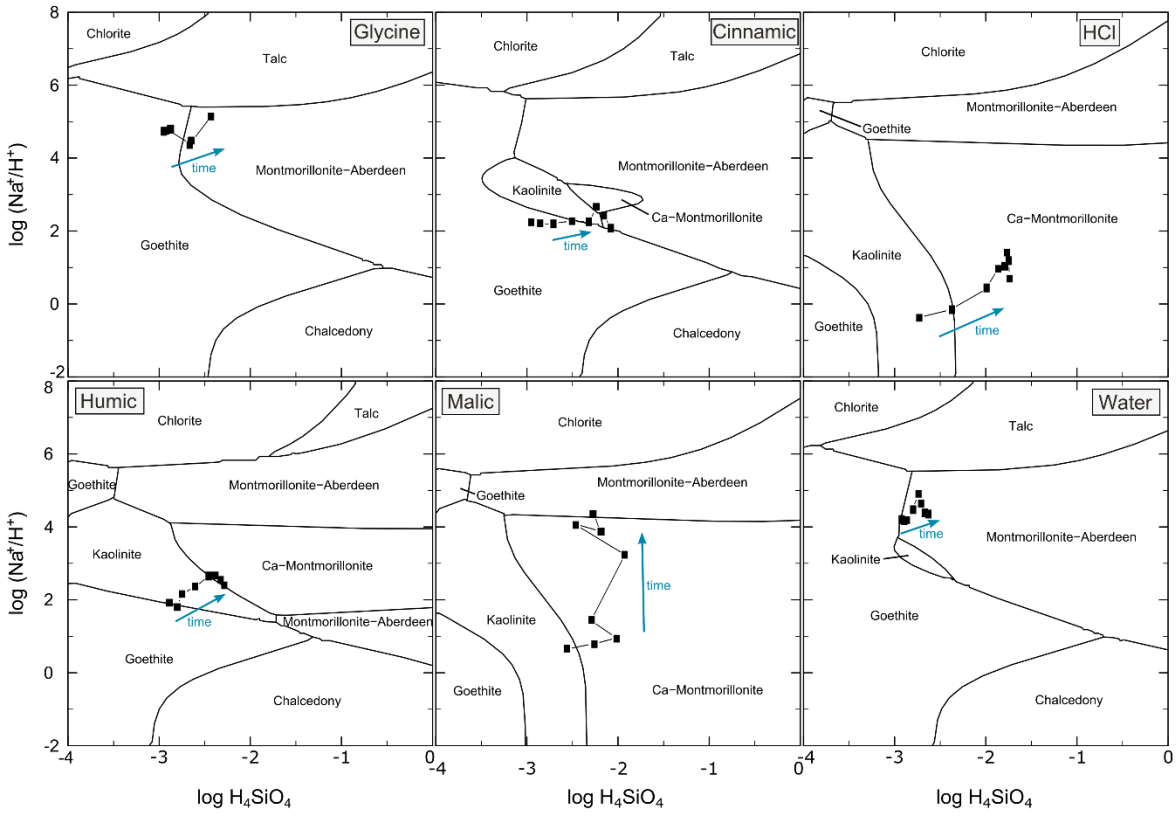

Figure 7. Mineral stability fields for all experiments calculated in the absence of hematite, which is supersaturated in all experimental solutions. The blue arrows marked “time” indicate the general direction of the chemical evolution in each experiment.

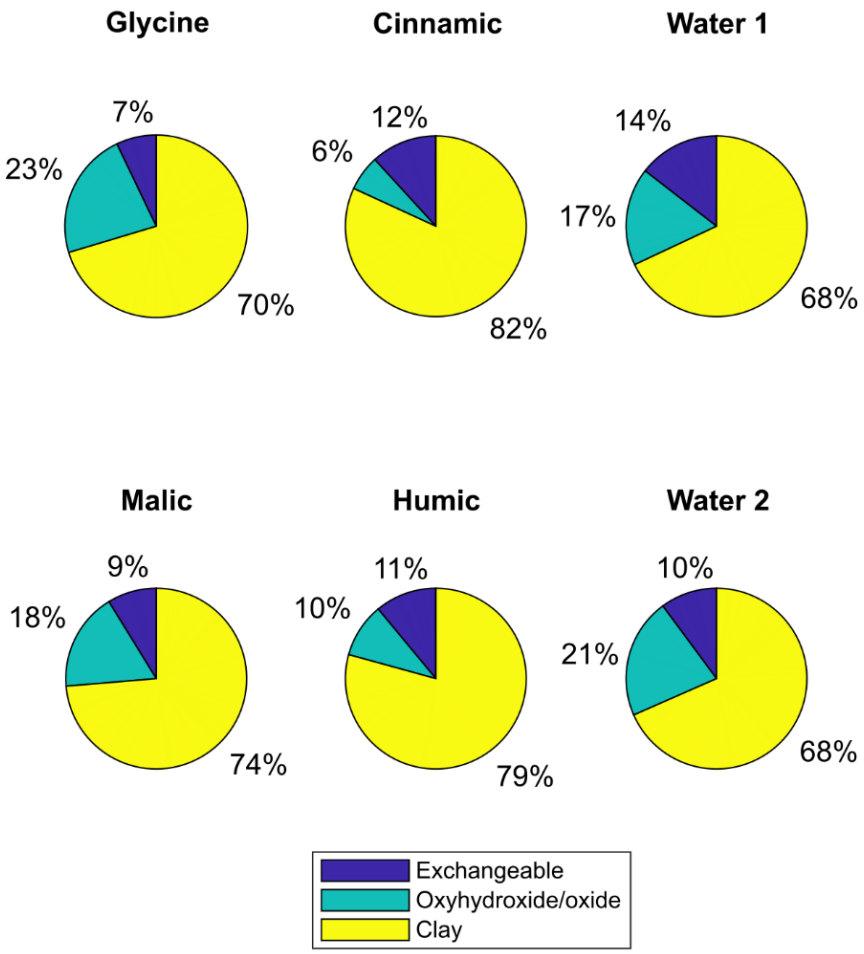

1047

1048 Figure 8. The Li mass balance for the post-experiment basalt, showing the proportions of Li

1049 taken from solution into the exchangeable, oxyhydroxide/oxide, and clay fractions,

1050 calculated by comparing each leach to the leach of the unreacted basalt.

1051

1052

1053

1054

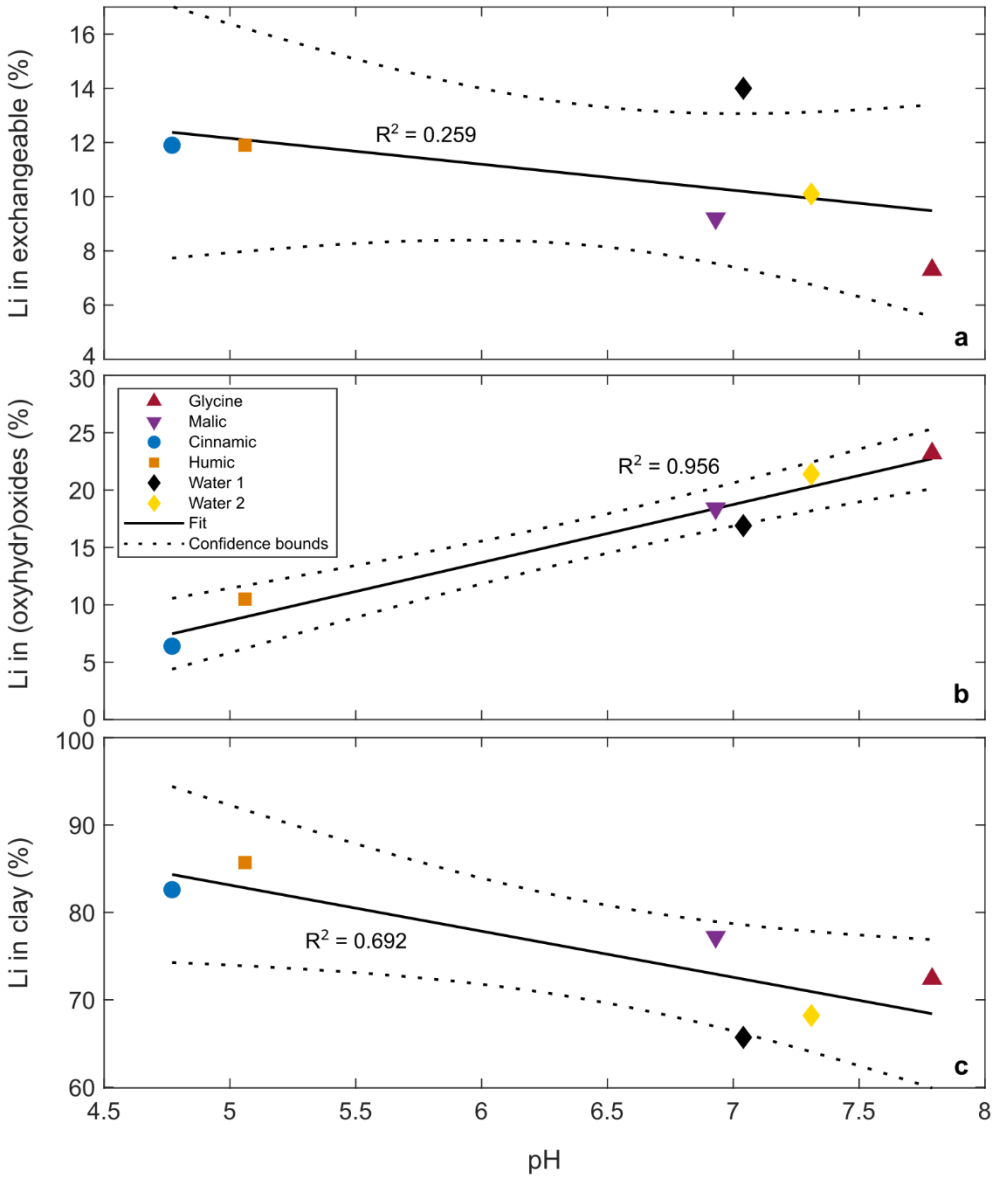

Figure 9. The proportions of Li in the (a) exchangeable, (b) oxide/oxyhydroxide, and (c) clay fractions of the post-experiment basalt, as a function of the final solution pH in each experiment.

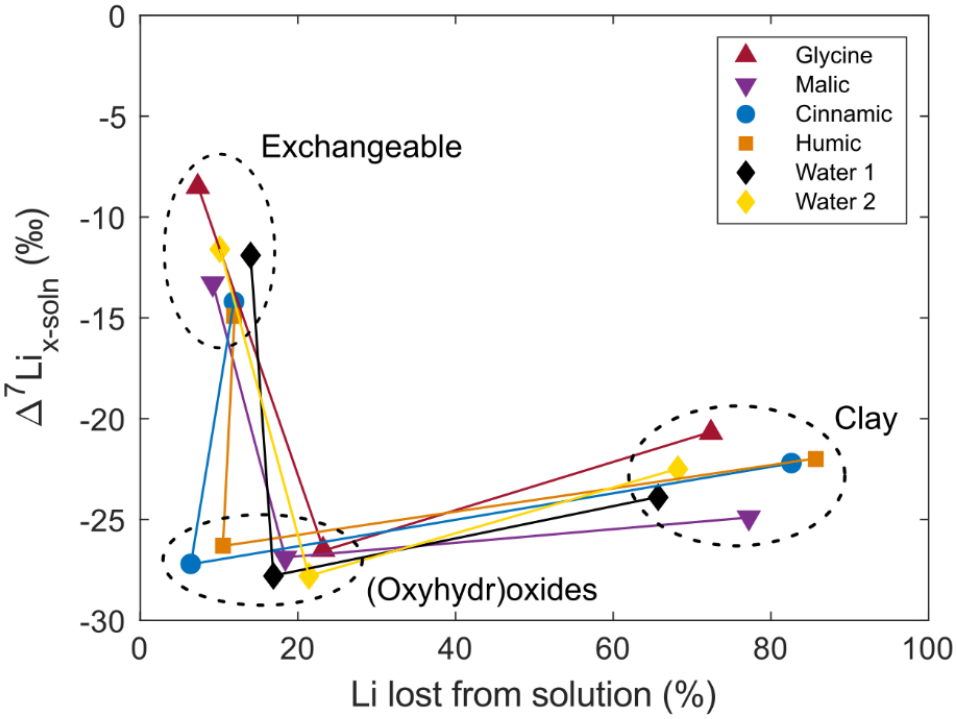

Figure 10. The destination of the Li lost from the solution of each experiment, as a function of the $\Delta^7Li_{x\text{-}soln}$, where "x" is the exchangeable, oxide/oxyhydroxide and clay fraction.

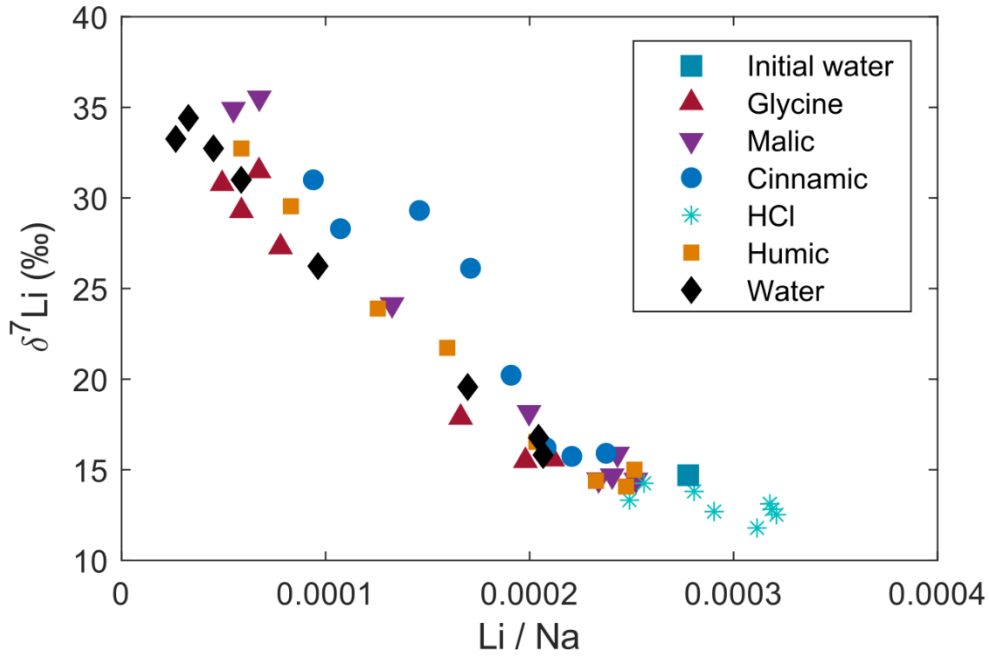

1078

1079

1080 Figure 11. Solution δ^7Li values as a function of Li/Na ratios. Note the negative co-variation in

1081 all the experiments, which is also observed in most natural basaltic surface waters due to

1082 the preferential removal of ^{6}Li into secondary phases.